Synthesis and SAR studies of novel 6,7,8-substituted 4-substituted benzyloxyquinolin-2(1*H*)-one derivatives for anticancer activity

Yi-Fong Chen [1,2], Yi-Chien Lin [2], Susan L. Morris-Natschke [3], Chen-Fang Wei [2], Ting-Chen Shen [2], Hui-Yi Lin [2], Mei-Hua Hsu [2], Li-Chen Chou [2], Yu Zhao [3], Sheng-Chu Kuo [1,2], Kuo-Hsiung Lee [3,4*], Li-Jiau Huang [1,2*]

[1] *The Ph.D. Program for Cancer Biology and Drug Discovery, China Medical University and Academia Sinica, No.91 Hsueh-Shih Road, Taichung, Taiwan*

[2] *School of Pharmacy, China Medical University, No.91 Hsueh-Shih Road, Taichung, Taiwan*

[3] *Natural Products Research Laboratories, UNC Eshelman School of Pharmacy, University of North Carolina, Chapel Hill, NC 27599-7568, USA*

[4] *Chinese Medicine Research and Development Center, China Medical University and Hospital, Taichung, Taiwan*

Correspondence:

Li-Jiau Huang, School of Pharmacy, China Medical University, no.91 Hsueh-Shih Road, Taichung, 40402, Taiwan. E-mail: ljhuang@mail.cmu.edu.tw or Kuo-Hsiung Lee, Natural Products Research Laboratories, UNC Eshelman School of Pharmacy, University of North Carolina, Chapel Hill, NC 27599-7568, USA. E-mail:

This article has been accepted for publication and undergone full peer review but has not been through the copyediting, typesetting, pagination and proofreading process, which may lead to differences between this version and the Version of Record. Please cite this article as doi: 10.1111/bph.12992

khlee@unc.edu

*Both authors contributed equally to this work.

BACKGROUND AND PURPOSE

4-Phenylquinolin-2(1*H*)-one (4-PQ) derivatives can induce cancer cell apoptosis. Additional new 4-PQ analogs were investigated as more effective, less toxic antitumor agents.

EXPERIMENTAL APPROACH

Forty-five 6,7,8-substituted 4-substituted benzyloxyquinolin-2(1*H*)-one derivatives were synthesized. Anti-proliferative activities were evaluated using an MTT assay, and structure-activity relationship correlations were established. Compounds **9b**, **9c**, **9e** and **11e** were also evaluated against the National Cancer Institute (NCI)-60 human cancer cell line panel. Hoechst 33258 and Annexin V-FITC/ PI staining assays showed that **11e** induced apoptosis of COLO 205 cells, while fluorescence microscopy experiments revealed inhibition of microtubule polymerization. Compound **11e**-treatment influenced expression of cell cycle- and apoptosis-related proteins in COLO 205 cells, causing G2/M arrest and multi-nucleation. Compound **11e** also increased levels of active caspase-3, -8, and -9 forms, but reduced procaspase-3, -8, -9, PARP, Bid, Bcl-xL, and Bcl-2.

KEY RESULTS

Nine 6,7,8-substituted-4-substituted-benzyloxyquinolin-2(1*H*)-one derivatives (**7e**, **8e**, **9b**, **9c**, **9e**, **10c**, **10e**, **11c** and **11e**) displayed high potency against HL-60, Hep3B, H460,

and COLO 205 cancer cells (IC_{50} <1 μM) without affecting Detroit 551 normal human cells (IC_{50} > 50 μM). Particularly, compound **11e** exhibited nanomolar potency against COLO 205 cancer cells. Mechanistic studies indicated that **11e** exerts anticancer effects by disrupting microtubule assembly and inducing G2/M arrest, polyploidy, and apoptosis via intrinsic and extrinsic signaling pathways. Activation of JNK might play a role in TRAIL-induced COLO 205 apoptosis.

CONCLUSION AND IMPLICATIONS

New quinolone derivatives were identified as potential pro-apoptotic agents. Compound **11e** should be used as a promising lead compound for future antitumor agent development.

Abbreviations

SAR, structure-activity relationship; NCI, National Cancer Institute; 4-PQ, 4-phenylquinolin-2(1*H*)-one; CDK, cyclin dependent kinase; CDKI, CDK inhibitors; BG, benzylguanine; AGT, alkylguanine-DNA alkyltransferase; pDOS, privileged-substructure-based diversity-oriented synthesis; PPA, polyphosphoric acid.

Introduction

Cancer is presently a worldwide health problem and leading cause of death in the United States and other developed countries (Rastogi *et al.*, 2004). Cancer is a formidable disease caused by disordered cell growth and invasion of tissues and organs. While various therapies and strategies have been developed to treat cancer, most of them have limitations. Thus, new anticancer drugs are continually needed. The main challenge facing clinical cancer therapy is to find a specific approach that kills malignant cells with no or few adverse effects on normal tissues, and considerable attempts have been made to develop innovative, safe and effective methods to defeat cancer. While scientists have discovered many agents with cytostatic action against cancer cells (Liu *et al.*, 2007; Folger *et al.*, 2011), increasing comprehension of the biological processes involved in cancer cell survival has led to the design and discovery of better targeted, novel therapeutic anticancer drugs. For several chemotherapeutic agents, a direct correlation has been found between antitumor efficacy and ability to induce apoptosis (Kaufmann *et al.*, 2000). Thus, approaches aimed at promoting apoptosis in cancer cells have gained paramount importance in future cancer research (Fesik, 2005; Fischer *et al.*, 2005).

Hetero-bicycles are indispensable structural units in compounds with a broad range of

biological activities. Among various nitrogen-containing fused heterocyclic skeletons, quinoline and quinolone structures are important components prevalent in a vast array of biological systems. Compounds with a quinoline nucleus exhibit various pharmacological properties, including antioxidant (Chung *et al.*, 2001; Zhang *et al.*, 2013), anti-inflammatory (Baba *et al.*, 1996; Mukherjee *et al.*, 2013), antibacterial (Cheng *et al.*, 2013), anti-HIV (Freeman *et al.*, 2004; Hopkins *et al.*, 2004), anti-malarial (Cornut *et al.*, 2013; Pandey *et al.*, 2013), anti-tuberculosis (Lilienkampf *et al.*, 2009), anti-Alzheimer's disease (Fiorito *et al.*, 2013), anticancer (Wang *et al.*, 2011; Abonia *et al.*, 2012; Chan *et al.*, 2012), etc. Accordingly, Soloman and Lee described quinoline-containing subunits as 'privileged structures' for drug development (Solomon *et al.*, 2011). 2-Quinolone [quinolin-2(1*H*)-one], also called 1-aza coumarin or carbostyril, and 4-quinolone are structural isomers. The 2-quinolone skeleton is a fertile source of biologically active compounds, including a wide spectrum of alkaloids investigated for antitumor activity (Ito *et al.*, 2004; He *et al.*, 2005; Nakashima *et al.*, 2012). In our previous investigation, 6,7-methylenedioxy-4-substituted phenylquinolin-2(1*H*)-one derivatives (4-phenylquinolin-2(1*H*)-ones; 4-PQs) were identified as novel apoptosis-inducing agents (Fig. 1) (Chen *et al.*, 2013b). Recently, Arya and co-workers reported that 4-hydroxyquinolin-2(1*H*)-one derivatives, prepared efficiently through microwave

irradiation, showed strong photo-antiproliferative activity (Arya *et al.*, 2007). Thus, we have directed our focus onto 4-PQ analogs as apoptosis stimuli. In our current study, we targeted the 2-quinolone structure as a basic scaffold of new derivatives with different substituents.

Purine-based compounds such as olomoucine and roscovitine (Fig. 1), which contain other hetero-bicyclic ring systems, are known ATP-binding site competitive inhibitors of cyclin dependent kinase (CDK) and are useful cell proliferation inhibitors in the treatment of cancer (Jorda *et al.*, 2011). Structure–activity relationship (SAR) studies on CDK inhibitors (CDKIs) demonstrated that a small hydrophobic group such as a non-polar benzyl group at the O^6- or N^6-position of the hetero-bicycle maximized CDK inhibition (Gibson *et al.*, 2002; Zatloukal *et al.*, 2013). In addition, numerous CDKI-related compounds that contain benzyl or arylmethyl groups on different core scaffolds, such as pyrazolo[1,5-*a*]pyrimidines (Paruch *et al.*, 2007), quinazolin-4-amines (Mott *et al.*, 2009), pyrimidine (Coombs *et al.*, 2013) and aminopurine (Doležal *et al.*, 2006) (Fig. 1), have been studied. Furthermore, a series of 6-(benzyloxy)-2-(aryldiazenyl)-9*H*-purine derivatives were reported to act as prodrugs of O^6-benzylguanine (O^6-BG; Fig. 1), which selectively targets O^6-alkylguanine-DNA alkyltransferase (AGT) in hypoxic tumor cells (Zhu *et al.*, 2013). The AGT protein plays a critical role in DNA repair, which can be

exploited in chemotherapeutic treatment of neoplastic cells (Dolan *et al.*, 1997; Daniels *et al.*, 2000). Alkylation of AGT with the benzyl group of O^6-benzylguanine (O^6-BG) results in complete depletion of the alkyltransferase protein. Consequently, numerous O^6-BG analogs have been developed as AGT inhibitors (Chae *et al.*, 1995; Terashima *et al.*, 1998). In 2008, Ruiz et al. (Ruiz *et al.*, 2008) reported that a family of quinolinone compounds acted as novel non-nucleosidic AGT inhibitors. These quinolinones could reach catalytic residue Cys145 buried deep within the binding groove, occupy the catalytic cleft of human DNA repair AGT protein, and act as substrate mimics of the O^6-guanine moiety.

Furthermore, the activity of biologically proven anticancer pharmacophores can be enhanced by introducing appropriate substitutions on the chemical scaffolds. In medicinal chemistry, shortening or lengthening chain length is a useful tactic to improve the affinity of target-binding. Some literature reports have demonstrated that the pro-apoptotic (antitumor) activity of certain compounds was dramatically improved by slightly changing the length and spacing of lateral branches, such as benzyl and other alkyl-aromatic side chains, on core skeletons (Al-Obaid *et al.*, 2009; Font *et al.*, 2011). Such exploration and utilization of chemical diversity relative to pharmacological space is an on-going drug discovery strategy, referred to as privileged-substructure-based

diversity-oriented synthesis (pDOS) (Oh *et al.*, 2011). Based on this strategy, as well as the structures shown in Fig. 1, we proposed addition of a substituted benzyl (C ring) side chain linked at the O^4-position of 4-hydroxyquinolin-2(1*H*)-one (2-quinolone scaffold) as a possible strategy for discovering new leads with pro-apoptotic bioactivity. The flexibility of the benzyl moiety might have some advantages to obtain better antitumor activity compared with our prior 4-PQ derivatives (Fig. 1). Therefore, we designed a series of 4-benzyloxyquinolin-2(1*H*)-one analogs **7a–e~15a–e**, with the general structures of target compounds depicted in Fig. 1. To the best of our knowledge, this is the first report on anticancer evaluation of 2-quinolone analogs bearing an O^4-benzyl moiety. The goal of current study is to discover more effective and less toxic antitumor agents, and contribute to the SAR profile of 2-quinolones with anti-proliferative activity and apoptotic induction in cancer cells.

Methods

Materials and physical measurements

All solvents and reagents were obtained commercially and used without further purification. The progress of all reactions was monitored by TLC (thin layer chromatography) on 2 × 6 cm pre-coated silica gel 60 F_{254} plates of thickness 0.25 mm

(Merck). The chromatograms were visualized under UV at 254–366 nm. Column chromatography was performed using silica gel 60 (Merck, particle size 0.063–0.200 mm). Melting points (mp) were determined with a Yanaco MP-500D melting point apparatus and are uncorrected. IR spectra were recorded on Shimadzu IR-Prestige-21 spectrophotometers as KBr pellets. The 1D nuclear magnetic resonance (NMR, ^{1}H and ^{13}C) spectra were obtained on a Bruker Avance DPX-200 FT-NMR spectrometer at room temperature. The 2D NMR spectra were obtained on a Bruker Avance DPX-400 FT-NMR spectrometer, and chemical shifts expressed in parts per million (ppm, δ). The following abbreviations are used: s, singlet; d, doublet; t, triplet; dd, double doublet; and m, multiplet. Mass spectra were performed at the Instrument Center of National Science Council at National Chung Hsing University, (Taichung City, Taiwan R.O.C.), using a Finnigan ThermoQuest MAT 95 XL (EI-MS).

*General procedure for the synthesis of 4-hydroxyquinolin-2(1H)-one derivatives (**5a-i**)*

4-Hydroxyquinolin-2(1*H*)-one derivatives **5a–i** were prepared by "one-pot" cyclization in polyphosphoric acid (PPA). A mixture of the appropriate substituted aniline **1a–i** (1 equiv) and diethylmalonate (**2**) (1.2 equiv) was heated with 5 – 6 times by weight PPA at 130 °C for 2 – 6 h (TLC monitoring). Then, the mixture was cooled and diluted with

water. A gum solidified upon standing overnight, and the precipitate was filtered, washed with water, and air-dried to provide **5a–i** with sufficient purity for the next reaction. Physical and spectroscopic data for **5a** are given below; the data for the remaining compounds are provided as Supplementary Material.

*4-Hydroxyquinolin-2(1H)-one (**5a**)(Mohamed, 1991; Nadaraj et al., 2006; Arya et al., 2007; Park et al., 2007; Zhang et al., 2008)*

Compound **5a** (3.48 g, 21.59 mmol)was obtained from aniline (**1a)** (3.82 g, 41.01 mmol) and diethylmalonate (**2**) (7.88 g, 49.20 mmol); yield: 53%; light-yellow solid; mp: 276–278 °C; IR(KBr) ν (cm^{-1}):1660 (C **=** O); ^{1}H NMR (200 MHz, DMSO-d_6) δ (ppm): 5.77 (s, 1H, H–3), 7.12 (t, *J* = 7.5 Hz, 1H, H–6), 7.26 (d, *J* = 8.2 Hz, 1H, H–8), 7.47 (t, *J* = 7.8 Hz, 1H, H–7), 7.77 (d, *J* = 8.0 Hz, 1H, H–5), 11.28 (br. s, 1H, NH); ^{13}C NMR (50 MHz, DMSO-d_6) δ (ppm): 98.56, 115.48, 115.63, 121.61, 123.11, 131.33, 139.55, 163.05, 164.18; MS (EI, 70 eV) *m/z*: 161.1$[M]^+$; HRMS (EI) *m/z*: calculated for $C_9H_7NO_2$: 161.0477; found: 161.0472.

*General procedure for the synthesis of 6,7,8-substituted-4-substituted benyloxyquinolin-2(1H)-one derivatives (**7a–e**, **8a–e**, **9a–e**, **10a–e**, **11a–e**, **12a–e**, **13a–e**, **14a–e**, **15a–e**)*

A mixture of 4-hydroxyquinolin-2(1*H*)-one derivatives **5a–i** (1 equiv) and K_2CO_3 (2

equiv) in DMF (10–20 mL) was heated at 90 °C for 1–2 h. The appropriate benzyl chloride or bromide (**6a–e**, 1–1.4 equiv) was added, and the mixture was heated at 80–90 °C for 1–6 h. Reaction completion was confirmed by TLC monitoring. The mixture was poured into ice water (200 mL), and the precipitated solid was collected by filtration and then washed with water. The residue was treated with EtOAc and purified by recrystallization. If no solid formed solids after addition of ice water, then the reaction mixture was extracted with EtOAc (3 × 100 mL). The combined organic layers were dried over anhydrous $MgSO_4$ before evaporation of solvent in vacuo. The residue was isolated by column chromatography (silica gel, EtOAc as eluate), and then recrystallized to give the corresponding pure products, 4-benzyloxyquinolin-2(1*H*)-one derivatives **7a–e**, **8a–e**, **9a–e**, **10a–e**, **11a–e**, **12a–e**, **13a–e**, **14a–e** and **15a–e**. Physical and spectroscopic data for **11e** are given as examples below; the data for the remaining compounds are provided as Supplementary Material.

*4-(3',5'-Dimethoxybenzyloxy)-6-methoxyquinolin-2(1H)-one (**11e**)*

Compound **11e** (0.70 g, 2.05 mmol) was obtained from **5e** (1.12 g, 5.86 mmol) and 3,5-dimethoxybenzyl bromide (1.48 g, 6.40 mmol); yield: 35%; white crystal; mp: 217–219 °C; IR (KBr) ν (cm^{-1}): 1674 (C = O); ^{1}H NMR (200 MHz, DMSO-d_6) δ (ppm): 3.74 (s,

6H, 3', 5'–OCH_3), 3.76 (s, 3H, 6–OCH_3), 5.20 (s, 2H, –O–CH_2–), 5.94 (s, 1H, H–3), 6.47 (dd, *J* = 2.2,2.2 Hz, 1H, H–4'), 6.66 (d, *J* = 2.2 Hz, 2H, H–2', H–6'), 7.14-7.26 (m, 3H, H–5,7,8), 11.32 (br. s, 1H, NH); ^{13}C NMR (50 MHz, DMSO-d_6) δ (ppm): 55.63 (2C), 55.78, 70.05, 98.71, 100.04, 104.17, 105.62 (2C), 115.50, 117.18, 120.50, 133.55, 138.76, 154.43, 161.07 (2C), 161.89, 163.23; MS (EI, 70 eV) *m/z*: 341.0 $[M]^+$; HRMS (EI) *m/z*: calculated for $C_{19}H_{19}NO_5$: 341.1263; found: 341.1257.

MTT assay for anti-proliferative activity

Human tumor cell lines of the cancer screening panel were maintained in RPMI-1640 medium supplemented with 10% fetal bovine serum (GIBCO/BRL), penicillin (100 U/mL)/streptomycin (100 μg/mL) (GIBCO/BRL) and 1% L-glutamine (GIBCO/BRL) at 37 °C in a humidified atmosphere containing 5% CO_2. Human hepatoma Hep 3B and normal skin Detroit 551 cells were maintained in DMEM medium supplemented with 10% fetal bovine serum (GIBCO/BRL), penicillin (100 U/mL)/streptomycin (100 μg/mL) (GIBCO/BRL) and 1% L-glutamine (GIBCO/BRL) at 37 °C in a humidified atmosphere containing 5% CO_2. Logarithmically growing cancer cells were used for all experiments. The human tumor cell lines were treated with vehicle or test compounds for 48 h. Cell growth rate was determined by MTT [3-(4,5-dimethylthiazol-2-yl)-2,5-

diphenyltetrazoliun bromide] reduction assay (Mosmann, 1983). After 48 h treatment, cell growth rate was measured on an ELISA reader at a wavelength of 570 nm and the IC_{50} values of test compounds were calculated.

In vitro NCI-60 human tumor cell line (HTCL) panel

In vitro cytotoxic activities were evaluated through the Developmental Therapeutic Program (DTP) of the National Cancer Institute (NCI) (Shoemaker, 2006). For more information on the anticancer screening protocol, please see: http://dtp.nci.nih.gov/branches/btb/ivclsp.html.

Cell morphology and Hoechst 33258 staining

COLO 205 cells were plated at a density of 2.5×10^5 cells per well in 12-well plates, and then incubated with 50 nM of compound **11e**for 12 h to 48 h. Cells were directly examined and photographed under a contrast-phase microscope. Nuclei were stained with Hoechst 33258 (bis-benzimide, Sigma) to detect chromatin condensation or nuclear fragmentation, features of apoptosis. After 0, 12, 24, 36, and 48 h, **11e**-treated cells were stained with 5 μg/mL Hoechst 33258 for 10 min. After washing twice with PBS, cells were fixed with 4% paraformaldehyde (PFA) in PBS for 10 min at 25 °C. Fluorescence of the soluble DNA (apoptotic) fragments was measured in a Varian Fluorometer at an

excitation wavelength of 365 nm and emission wavelength of 460 nm.

Apoptosis studies

Determination of apoptotic cells by fluorescent staining was done as described previously (van Engeland *et al.*, 1998; Zhuang *et al.*, 2013). The Annexin V-FITC Apoptosis Detection Kit was obtained from Strong Biotech Corporation (Strong Biotech, Taiwan). The COLO 205 cells (2×10^5 cells/well) were fluorescently labeled for detection of apoptotic and necrotic cells by adding 100 μL of binding buffer, 2 μL of annexin V-FITC, and 2 μL of PI to each sample. Samples were mixed gently and incubated at room temperature in the dark for 15 min. Binding buffer (300 μL) was added to each sample immediately before flow cytometric analysis. A minimum of 10,000 cells within the gated region was analyzed.

Flow cytometric analysis for cell cycle

COLO 205 cells were added to 50 nM of **11e** for 0 h, 12 h, 24 h, 36 h, and 48 h. Cells were fixed in 70% EtOH overnight, washed twice, and re-suspended in PBS containing 20 μg/mL PI, 0.2 mg/ml RNase A, and 0.1% Triton X-100 in the dark. After 30 min incubation at 37 °C, cell cycle distribution was analyzed using ModFit LT Software (Verity Software House, Topsham, USA) in a BD FACSCanto flow cytometer (Becton

Dickinson, San Jose, CA).

Molecular modeling

The crystal structure of microtubules in complex with *N*-deacetyl-*N*-(2-mercaptoacetyl)-colchicine (DAMA-colchicine) was downloaded from the Protein Data Bank (PDB entry 1SA0 : http://www.rcsb.org/pdb/home/home.do) (Ravelli *et al.*, 2004). Docking studies were performed for proposed **11e** in the colchicine binding site of tubulin. The AutoDock Vina was used to perform docking calculations (Trott *et al.*, 2010). The final results were prepared with PyMOL (v. 1.3) in Windows 7. After removing the ligand and solvent molecules, hydrogen atoms were added to each amino acid atom. The 3D structure of compound were obtained from ChemBioDraw ultra 12.0 followed by MM2 energy minimization. Docking was carried out by AutoDock Vina in the colchicine binding pocket. Grid map in AutoDock 4.0 was used to define the interaction of protein and ligand in the binding pocket. For compound binding into the colchicine binding site, a grid box size of 25×25×25 points in x, y and z directions was built and the grid center was located in x = 116.909, y = 89.688, and z = 7.904.

Localization of microtubules

After treatment, cells were fixed with 4% paraformaldehyde (PFA) in PBS, blocked with

2% bovine serum albumin, stained with anti-tubulin monoclonal antibody, and then with FITC conjugated anti-mouse IgG antibody. PI was used to stain the nuclei. Cells were visualized using a Leica TCS SP2 Spectral Confocal System.

Mitochondrial membrane potential analysis

Cells were plated on 6 well at 1.0×10^6 cells/well and treated with 50 nM **11e** for 6–24 h. Mitochondrial membranes were stained with 0.5 ml JC-1 working solution (BD MitoScreen Kit) added to each sample. Samples were incubated for 10–15 min at 37 °C in the dark. Mitochondrial membrane potential was measured using the BD FACSCanto flow cytometer (Becton Dickinson, San Jose, CA).

Western blot assay

The treated cells (1×10^7 cells/10 mL in 10 cm dish) were collected and washed with PBS. After centrifugation, cells were lysed in a lysis buffer. The lysates were incubated on ice for 30 min and centrifuged at 12000 *g* for 20 min. Supernatants were collected, and protein concentrations were then determined using Bradford Assay. After adding a 5× sample loading buffer containing 625 mM Tris-HCl, pH = 6.8, 500 mM dithiothreitol, 10% SDS, 0.06% bromophenol blue, and 50% glycerol, protein samples were electrophoresed on 10% SDS-polyacrylamide gel, and transferred to a nitrocellulose

membrane. Immunoreactivity was detected using the Western blot chemiluminescence reagent system (PerkinElmer, Boston, MA).

Statistical analysis

Statistical analysis was performed with an analysis of variance (ANOVA) followed by Tukey's test. All data were expressed as mean ± SEM. *$P < 0.001$ was indicative of a significant difference.

Results

Chemistry

The synthetic procedures for the new 4-substituted benzyloxyquinolin-2(1*H*)-ones (**7a–e~15a–e**) are illustrated in Scheme 1. A general synthetic approach to the key intermediate 4-hydroxyquinolin-2(1*H*)-one is the Knorr quinoline synthesis, which involves cyclization and dehydration of a transient β-ketoanilide, formed by condensation of a β-ketoester and aniline at relatively high temperature. More specific synthetic approaches include cyclization of *N*-acetylanthranilic acid derivatives (Buckle *et al.*, 1975), condensation of malonates/malonic acid with anilines using $ZnCl_2$ and $POCl_3$ (Zhang *et al.*, 2008; Priya *et al.*, 2010), Ph_2O (Ahvale *et al.*, 2008), and cyclization

of malonodianilides with polyphosphoric acid (PPA) (Cai *et al.*, 1996; Park *et al.*, 2007; Moradi-e-Rufchahi, 2010), CH_3SO_3H/P_2O_5 (Kappe *et al.*, 1988), *p*-toluenesulfonic acid (Nadaraj *et al.*, 2006). In our study, 4-hydroxyquinolin-2(1*H*)-one derivatives (**5a–i**) were synthesized by treatment of a substituted aniline (**1a–i**) with diethylmalonate (**2**) in one-flask (Mohamed, 1991; Arya *et al.*, 2007), followed by cyclization of the formed monoanilide (**3a–i**) or malondianilide (**4a–i**) precursors in the presence of PPA. The target 4-benzyloxyquinolin-2(1*H*)-one derivatives **7a–e**, **8a–e**, **9a–e**, **10a–e**, **11a–e**, **12a–e**, **13a–e**, **14a–e** and **15a–e** were synthesized by reaction of the intermediate 4-hydroxyquinolin-2(1*H*)-one derivatives **5a–i** with various benzyl halide **6a–e** in the presence of K_2CO_3 and DMF (Guo *et al.*, 2009; Deng *et al.*, 2010). All synthetic products were characterized by IR, ^{1}H and ^{13}CNMR, and mass spectroscopy.

Previous literature has reported that 2-quinolones have a minor tautomeric structure (2-hydroxyquinoline) due to protonation of the carbonyl oxygen (Lewis *et al.*, 1991). Deprotonation of the 2-quinolonewould cause ring resonance and electron shifting within the *N*-1, *O*-2, *C*-3 and *O*-4 positions of the 4-hydroxyquinolin-2(1*H*)-one derivatives (Fig. 2A) (Pirrung *et al.*, 1999). Consequently, previous reports have indicated that 4-hydroxyquinolin-2(1*H*)-ones could be alkylated at the 1-*N*H, 2-*O*H, 4-*O*H, or 3-*C*H position (Park *et al.*, 2004; Ahmed *et al.*, 2010; Ahmed *et al.*, 2011). Therefore, we

confirmed the structures of our synthesized compounds using NMR spectroscopic analyses. The ^{1}H NMR spectrum of 4-benzyloxyquinolin-2(1*H*)-one derivatives **7a–e~15a–e** featured a singlet for *O*-linked C(9)-H_2 methylene protons between 5.13–5.27 ppm, a singlet for a C(3)-*H* proton between 5.80–6.09 ppm, and a broad singlet for an exchangeable N*H* group between 10.47–11.54 ppm. The chemical shifts for the benzylic CH_2 were consistent with *O*-alkylation rather than *N*-alkylation (Park *et al.*, 2004). The ^{13}C shifts for *O*-alkylated compounds are typically downfield (higher ppm value; 52.7–68.4) compared with *N*-alkylated compounds (lower ppm value; 28.6–45.0) (LaPlante *et al.*, 2013). The ^{13}C NMR spectra of **7a–e~15a–e** included a *O*-linked methylene carbon between 65.74–70.74 ppm, which again indicated *O*-alkylation. Furthermore, regioselective alkylation at the 4-*O*H position was confirmed by two-dimensional NMR study via heteronuclear multiple-quantum correlation (HMQC) and heteronuclear multiple-bond correlation (HMBC) spectroscopy experiments that disclose the relationship between ^{1}H–^{13}C coupling. In the case of compound **11e**, as shown in Fig. 2B, the 4-*O*-linkage was supported by observation of ^{3}J-HMBC correlations between C(9)-*H* methylene protons (δ_H 5.20) on the 3',5'-dimethoxybenzyloxy moiety with the carbon at *C*(4) position (δ_c 161.89) of the 2-quinolone core, which shows a further correlation with the C(5)-*H* proton (δ_H 7.14–7.26, overlapped). In other words, O^4-alkylation was

determined through the observation of H9/C4 and H5/C4 crosspeaks. These data proved that 3',5'-dimethoxybenzyloxy moiety is attached to the 4-*O*-position of the 2-quinolone core-structure. Furthermore, the IR spectra of **7a–e~15a–e** possessed a characteristic absorption band for an amido C **=** O group (1633–1674 cm^{-1}).

Biological evaluation and structure-activity relationship (SAR) analysis

All newly synthesized target compounds (**7a–e**, **8a–e**, **9a–e**, **10a–e**, **11a–e**, **12a–e**, **13a–e**, **14a–e** and **15a–e**) were assayed for growth inhibitory activity against Detroit 551 (human normal skin fibroblast) and four cancer cell lines, including HL-60 (leukemia), Hep 3B (hepatoma), H460 (non-small-cell-lung carcinoma) and COLO 205 (colorectal adenocarcinoma). Cells were treated with compounds for 48 h, and cell proliferation was determined by 3-(4,5-dimethylthiazol-2-yl)-2,5-diphenyltetrazoliun bromide (MTT) assay. The antiproliferative activity of each compound was presented as the concentration of compound that achieved 50% inhibition (IC_{50}) of cancer cell growth. The results are summarized in Table 1. Collectively, the present series of novel 4-benzyloxyquinolin-2(1*H*)-one derivatives exhibited diverse potency against the four tested tumor cell lines. Among them, compounds **7e**, **8e**, **9b**, **9c**, **9e**, **10c**, **10e**, **11c** and **11e** displayed high potency against HL-60, Hep3B, H460 and COLO 205 cells, with IC_{50}

value less than 1 μM (Table 1). Notably, **11e** displayed the most prominent growth inhibitory activities against the above cell lines with IC_{50} values ranging from 14 to 40 nM. Moreover, none of the active compounds showed cytotoxicity toward Detroit 551 (IC_{50} > 50 μM) cells. These results suggested that this new series of 4-benzyloxyquinolin-2(1*H*)-one derivatives could effectively suppress tumor growth without causing toxicity to normal somatic cells.

Based on the obtained biological data, SAR correlations were determined. Firstly, we evaluated the effects of methoxy-substitution of the *C*-4 benzyloxy ring (C ring) on the cytotoxic activity. Generally, compounds with 3',5'-dimethoxybenzyloxy side chain (**7e–15e**) showed the highest potency in their respective series (**7–15**). Among them, compounds **7e**, **8e**, **9e**, **10e** and **11e** exhibited significant activity against Hep 3B, H460 and COLO 205 cancer cell lines (IC_{50} < 1 μM). These results indicated 3',5'-dimethoxy-benzyloxy substitution is preferred relative to other benzyl substitution. Compounds **9b**, **9c**, **10b**, **10c**, **11b**, **11c** with a 2'- or 3'-methoxybenzyloxy side chain demonstrated moderate activity (IC_{50} 0.2 – 5.0 μM), whereas compounds bearing side chains of benzyloxy or 4'-methoxybenzyloxy were inactive (IC_{50} > 50 μM) or exhibited only marginal activity (IC_{50} 4.5 – 10μM).

Next, we explored the SAR of the 2-quinolone A-ring. Compounds with a substituted

benzyloxy moiety at *C*-4 and various functional groups at *C*-6, -7 and -8 were studied, and different anticancer effects were found. Regarding the *C*-6 substitution, compound **8e** (6-fluoro), **9e** (6-chloro), **10e** (6-methyl) and **11e** (6-methoxy) were more potent than **7e** (no substitution). Moreover, compound **11e** (IC_{50} 0.014–0.04 μM) displayed the strongest growth inhibitory activity among the *C*-6 substituted compounds, suggesting that the *C*-6 methoxy group might play a pivotal role. Moving the methoxy group from *C*-6 to *C*-7 (**12e**, IC_{50} 2.11–4.9 μM) or *C*-8 (**13e**, IC_{50} 2.2–3.8 μM) led to dramatically decreased inhibitory activity. Activity also decreased when the *C*-8 methoxy of **13e** was replaced with chlorine (**14e**), while activity was retained when the methoxy was replaced with methyl (**15e**). Thus, in this series of 4-benzyloxy-2-quinolones, optimal anti-proliferative effects were found with a 6-methoxy group on the 2-quinolone ring.

In the present work, the above findings can be summarized in the following two SAR conclusions:

1. The *in vitro* anticancer activity of the substituted benzyloxy moiety (C ring) on the 4-position of 2-quinolone derivatives can be ranked in the following order of decreasing activity: 3',5'-dimethoxybenzyloxy (**7e–15e**) > 3'-methoxybenzyloxy (**7c–15c**) ≥ 2'-methoxybenzyloxy (**7b–15b**) > benzyloxy (**7a–15a**) ≥ 4'-methoxybenzyloxy (**7d–15d**).

2. C-6 substituents on the 2-quinolone (A ring) resulted in better activity compared with C-7 and C-8 substituent. The following rank order of in vitro anticancer activity was found relative to the identity of the C-6 substituent: 6-methoxy > 6-chloro > 6-methyl > 6-fluoro > no substitution.

*Anticancer drug screen panel of compound **9b**, **9c**, **9e** and **11e** against NCI-60 human cancer cell lines*

We selected four potent compounds **9b**, **9c**, **9e** and **11e** and submitted them for screening against the NCI-60 HTCL panel assay through the US NCI Developmental Therapeutics Program (Boyd *et al.*, 1995; Shoemaker, 2006). The cell lines represent nine tumor subpanels, leukemia, melanoma and cancers of lung, colon, brain (CNS), ovary, kidney, prostate and breast. Initially, the compounds were added at a single dose (10 μM) and the culture incubated for 48 h. End point determinations were made with a SRB (sulforhodamine B) assay. Results for each compound are given in Table 2, with a negative value in the cell growth percentage indicating an anti-proliferative effect against that cell line. Compound **9b** displayed positive cytotoxic effects toward 11 out of 60 cell lines, and the positive cytotoxic proportions of **9c**, **9e**, and **11e** were 10/59, 18/60, and 26/57. Our prominent compound **11e** exhibited inhibitory effects ranging from –59.50%

to –0.80%. At the primary single high dose 10 μM (10^{-5} M), **9b**, **9c**, **9e**, and **11e** showed greatest effects against colon carcinoma COLO 205 with cell growth percentage of –55.40, –57.40, –64.41, and –59.50, respectively. The melanoma MDA-MB-435 cell line was also sensitive to these compounds (growth percentages –46.28%, –43.14%, –43.16%, and –41.44%, respectively).

At the second evaluation stage, the selected compounds were evaluated at five different concentrations (0.01, 0.1, 1, 10, and 100 μM) against same NCI-60 HTCL panel. The outcomes were represented by three calculated response parameters (GI_{50}, TGI, and LC_{50}) for each cell line through growth percent inhibition curves (Holbeck, 2004; Holbeck *et al.*, 2010). The GI_{50} value (growth inhibitory activity) corresponds to the concentration of compound causing 50% decrease in net cell growth, the TGI value (cytostatic activity) is the concentration of compound resulting in total growth inhibition (100% growth inhibition) and LC_{50} value (cytotoxic activity) is the lethal dose of compound causing net 50% death of initial cells. The calculated results are presented as log concentration (given in supplementary data), as shown in Table 3. The NCI data revealed broad-spectrum sensitivity profiles for **9b**, **9c**, **9e** and **11e** toward all nine cancer subpanels with GI_{50} values less than 1 μM, and less than 0.01 μM ($\log GI_{50} < -8.0$) against some cell lines for **9e** and **11e**. The anticancer effects of these compounds were

comparable to those of fluorouracil (5-FU), which is widely used clinically for treating malignancy (Longley *et al.*, 2003). These screening results correspond with the one single dose results, showing broad anticancer spectra for **9b**, **9c**, **9e** and **11e**. Notably, prominent compound **11e** exhibited GI_{50} values ranging from 0.01 to 8.08 μM in 51 of the 56 cell lines, with GI_{50} values below 0.01 μM in five cell lines (leukemia K-562 and SR, non-small cell lung cancer NCI-H522, colon cancer COLO 205, melanoma MDA-MB-435).

To further determine which cancer subtypes were more sensitive to these 4-benzyloxy-2-quinolones, we calculated subpanel-selectivity ratios based upon GI_{50} values. The calculated results are shown in Table 4 and Fig. 3. Selectivity ratios less than 3 were rated non-selective, ratios ranging from 3 to 6 were termed moderately selective, and ratios greater than 6 were designated highly selective (Boyd *et al.*, 1995; Noolvi *et al.*, 2012; Chen *et al.*, 2013a). With all ratios less than 3, compounds **9b** and **9c** were rated non-selective toward all nine subpanels. Interestingly, both **9e** and **11e**, which contain a 3',5'-dimethoxybenzyloxy moiety, were much more selective than **9b** and **9c** (Fig. 3). As shown in Table 4, the average selectivity ratios of **9e** and **11e** (ratios = 6.51 and 4.05) were higher than those of **9b** and **9c** (ratios = 1.12 and 1.28). Compound **9e** exhibited selectivity against leukemia, colon cancer, CNS cancer, melanoma, renal cancer and

prostate cancer with selectivity ratios of 7.56, 9.09, 10.28, 10.00, 7.89 and 8.57, respectively. Regarding total MID, the most prominent compound **11e** displayed significant activity (0.31 μM) and was moderately selective toward the breast cancer subpanel with a selectivity ratio of 3.83 and highly selective against leukemia, colon cancer and prostate cancer with selectivity ratios of 7.36, 10.42, and 10.42, respectively. Among the subpanels rated highly selective, colon cancer was extremely sensitive to compound **11e** (NSC 764592; Fig. 3). This compound showed exceptional potency against the individual cell line COLO 205 (LC_{50} 0.09 μM, TGI 0.03 μM) (Table 3). From the dose-response curves against six colon cancer cell lines (Fig. 4), it is also obvious that **11e** exhibited unique selectivity against COLO 205.

*Morphological changes and apoptosis in COLO 205 cells induced by compound **11e***

Based on the in vitro cytotoxicity data, **11e** (NSC 764592), the most potent compound against COLO 205 cells, was selected for further biological studies. Apoptosis is well known as a process of programmed cell death (cell suicide) (Elmore, 2007). In our previous study, 4-phenyl-2-quinolone analogs (4-PQs) could induce cell cycle arrest and apoptosis in both HL-60 and H460 cells (Chen *et al.*, 2013b). In order to characterize the cellular basis for the antiproliferative effects of selected derivative **11e**, we investigated

the compound's apoptosis inducing ability in COLO 205 cells. Morphological analysis confirmed the cytotoxic effects of **11e**. As shown in Fig. 5A, the apoptotic morphological changes included cell rounding and shrinkage after 24 h incubation with 50 nM of **11e** (the black arrowhead indicates an apoptotic nucleus). To confirm the induction of apoptosis by **11e**, COLO 205 cells were stained with Hoechst 33258, a fluorescent DNA-staining dye, and cell morphology was investigated using fluorescence microscopy. As shown in Fig. 5B, control cells exhibited uniformly dispersed chromatin, homogeneous blue fluorescence in the nuclei, normal organelles, and intact cell membranes. In cells treated with 50 nM of **11e** for 24, 36, and 48 h, the nuclei budded off into several fragments, and nuclear condensation and fragmentation were observed (Fig. 5B), indicating typical characteristics of apoptosis, including condensation of chromatin, shrinkage of nuclei, and appearance of apoptotic bodies (the black arrowhead indicates an apoptotic nucleus).

Annexin V-FITC/PI double-labeling was used to detect phosphatidylserine (PS) externalization, a hallmark of apoptosis (van Engeland *et al.*, 1998; Zhuang *et al.*, 2013). In Fig. 5C, populations of viable (annexin V−, PI−), early apoptotic (annexin V+, PI−), late apoptotic (annexin V+, PI+) and necrotic (annexin V−, PI+) cells are found in quadrants (Q) 3, 4, 2, and 1, respectively. Cells incubated in the absence of **11e** were

undamaged and stained with negative for annexin V-FITC and PI (Q3). After incubation with 50 nM of **11e**, the number of early apoptotic cells stained positive by annexin V-FITC and negative with PI (Q4) increased significantly with incubation time, from 5.5% (control) to 7.7% after 12 h, 12.7% after 24 h, 20.9% after 36 h, and 21.8% after 48 h incubation. The number of late apoptotic cells stained positive by annexin V-FITC and PI (Q2) also increased with incubation time, from 9.9% (control) to 10.2% after 12 h, 10.4% after 24 h, 8.6% after 36 h, and 16.1% after 48 h incubation. Thus, when COLO 205 cells were stained with Annexin-V/PI and analyzed with flow cytometry, early and late apoptotic (Annexin-V-stained) cells increased in a time-dependent manner (Fig. 5C), which indicates that **11e** can induce apoptosis.

*Toxicity of COLO 205 cells induced by **11e***

Exposure of COLO 205 cells to **11e** for 48 h, followed by MTT metabolism assays, confirmed the effects of **11e** on cell viability. The IC_{50} value was 27.2 ± 1.4 nM, and **11e** reduced COLO 205 cell viability in a dose-dependent manner. Exposure of COLO 205 cells to 10, 25, 50, 75, and 100 nM **11e** reduced the survival to 86.3 ± 0.6%, 49.3 ± 1.4%, 22.4 ± 0.3%, 19.2 ± 0.5%, and 18.7 ± 1.2%, respectively, of the control (0.1% DMSO) (Fig. 6B). Compound **11e** inhibited COLO 205 cell growth in dose- and time-dependent

manners (Fig. 6C).

11e *induced apoptotic cell death and interfered with cell-cycle distribution in G2/M phase arrest*

COLO 205 cells were treated with 50 nM of **11e** for 0, 6, 12, 24, 36, and 48 h, followed by flow cytometry analysis to determine the cell cycle distribution of treated cells, as well as to investigate the **11e**-induced inhibition of COLO 205 cell growth by cell cycle arrest and apoptotic mechanisms. As shown in Fig. 7A, **11e** induced a time-dependent accumulation of G2/M cells (11.72% G2/M at 0 h; 33.76% G2/M at 6 h; 58.98% G2/M at 12 h; 90.43% G2/M at 24 h; 82.82% G2/M at 36 h; 59.99% G2/M at 48 h), and apoptotic (sub-G1) cells (0.32% sub-G1 at 0 h; 1.29% sub-G1 at 6 h; 1.91% sub-G1 at 12 h; 7.18% sub-G1 at 24 h; 26.15% sub-G1 at 36 h; 45.56% sub-G1 at 48 h). The results showed that **11e** disturbed the cell-cycle process and induced COLO 205 cell death through an increase in the sub-G1 phase.

11e *inhibits microtubule polymerization in COLO 205 cells*

COLO 205 cells were treated with **11e** (50 nM) for 24 h and then visualized using confocal microscopy to investigate the effects of **11e** on microtubule function. As shown in Fig. 7B, treatment with **11e** resulted in microtubule changes similar to those

induced by colchicine. Both compounds caused cellular microtubule depolymerization with short microtubule fragments scattered throughout the cytoplasm. In contrast, taxol significantly increased tubulin polymerization.

Molecular modeling and computational studies

Using a molecular docking method and molecular mode of tubulin and *N*-deacetyl-*N*-(2-mercaptoacetyl)-colchicine (DAMA-colchicine), **11e** was docked into the colchicine-binding domain of tubulin. As shown in Fig. 8A and B, **11e** inserted deeply into the colchicine-binding pocket of α- and β-tubulin, very similar to the binding mode of DAMA-colchicine. Superimposition of compounds in the colchicine-binding site indicated that ring C and ring A are comparable pharmacophores between DAMA-colchicine and **11e** (Fig. 8C and 8D). As shown in Fig. 8D, the 1-NH group of **11e** overlapped with the acetamide-NH group of DAMA colchicine. Moreover, the 1-NH of **11e** formed a hydrogen bond with Thr179α as was also observed with the acetamide-NH group of DAMA-colchicine. The -O-CH_2- group of **11e** occupied a region in space in proximity to the C5 and C6-positions in the B-ring of DAMA colchicine and was involved in hydrophobic interactions with Lys254β, Ala250β, and Leu248β. The 3',5'-dimethoxy of **11e** overlapped with the 1,3-dimethoxy moiety in the

C ring of DAMA-colchicine, the C-ring was involved in hydrophobic interactions with Leu255β. Finally, the quinolin-2(1*H*)-one scaffold of **11e** partly overlapped with the A-ring of DAMA-colchicine and formed hydrophobic interactions with Asn258β and Lys352β.

***11e** changes the expression and phosphorylation status of G2/M regulatory proteins in COLO 205 cells*

Analysis of cell cycle-related protein expression explored the mechanisms by which **11e** induces G2/M arrest. Firstly, COLO 205 cells treated with 50 nM of **11e** showed increased cyclin B1 and CDK1 protein levels, which are markers for induction of mitotic arrest (Fig. 9A). Secondly, given the importance of the Aurora kinases in cancer cell mitosis and metastasis, the effects of **11e** (50 nM in COLO 205 cells) on aurora kinase function were investigated. As shown in Fig. 9B, **11e** decreased aurora A, phospho-aurora A, aurora B, and phospho-aurora B expression. Thirdly, we examined whether **11e** inhibited phosphorylation of histone H3 in COLO 205 cells. Histone H3 is one substrate of aurora B kinase. During mitosis, aurora-B is required for phosphorylation of histone H3 on serine 10, which might be important for chromosome condensation (Keen *et al.*, 2004). As shown by using Western blot

analysis, **11e** decreased phospho-H3 expression after a 6 h treatment (Fig. 9B). This finding suggests that inactivation of aurora kinases A and B is involved in **11e**-induced G2/M arrest.

***11e**-induced apoptosis associated with caspase-3, caspase-8, caspase-9, and PARP cleavage*

To confirm the possibility that **11e**-induced apoptosis is related to contributions from the intrinsic or extrinsic signal pathway, COLO 205 cells were treated with 50 nM of **11e** for 6, 12, 24, 36, and 48 h, and then the activities of caspase-3, caspase-8, and caspase-9 were determined using a Western blot assay. As shown in Fig. 10, **11e** induced significant caspase-3, caspase-8, and caspase-9 activity. Results from the Western blot assay also indicated that **11e** induced PARP cleavage, which is an important apoptosis marker. PARP is cleaved by caspase-3 between Asp214 and Gly215 to yield p85 and p25 fragments.

*Intrinsic apoptotic pathway proteins are modulated during **11e**-induced apoptosis*

The mitochondria are key organelles in the control of apoptosis. Accordingly, we investigated whether **11e** was capable of inducing depolarization of the mitochondrial membrane potential ($\Delta\psi$m) using JC-1, a lipophilic fluorescent cation that incorporates

into the mitochondrial membrane. COLO 205 cells were treated with 50 nM of **11e** for 6, 12, 24, 36, and 48 h, followed by staining with JC-1, to confirm apoptosis as the cause of decreased $\Delta\psi$m. As shown in Fig. 11A, in healthy cells with high mitochondrial $\Delta\psi$m, JC-1 spontaneously formed complexes known as JC-1 polymer (P2), which showed intense red fluorescence (0 h). Over time, the percentage of cells with reduced red fluorescence (P3) showed a significant increase. This effect is indicative of a change in $\Delta\psi$m in the population in which apoptosis was induced (6–36 h). Moreover, it is well known that the dissipation of $\Delta\psi$m causes release of cytochrome *c*, Apaf-1, apoptosis-inducing factor (AIF), and Endo G into the cytosol, with consequent activation of the execution phase of apoptosis. In this study, we also demonstrated that mitochondrial cytochrome *c*, Apaf-1, AIF, and Endo G were released into the cytosol during **11e**-induced apoptosis (Fig. 11B).

Bcl-2 family proteins are key regulators of mitochondrial-related apoptotic pathways (Zhai *et al.*, 2008; Roy *et al.*, 2014). Some of these proteins, such as Bcl-2 and Bcl-xL, are anti-apoptotic (pro-survival) proteins, whereas others, such as Bad, Bax, and Bid, are pro-apoptotic proteins. The Bcl-2 and Bcl-xL proteins located in the outer mitochondrial membrane are necessary for maintaining mitochondrial integrity. Furthermore, phosphorylation is a common characteristic of destabilized mitochondria.

The balance of pro- and anti-apoptotic Bcl-2 proteins influences the sensitivity of cells to apoptotic stimuli (Brunelle *et al.*, 2009). Previous research has shown that an increase in the ratio of Bax/Bcl-2 within a cell predisposes it to certain apoptotic stimuli. Bax and Bak induce the release of cytochrome *c* and loss of mitochondrial membrane potential, whereas Bcl-2 and Bcl-xL inhibit these effects. Because **11e** results in caspase-9 activation, which is also a mitochondria-mediated caspase, we sought to determine whether **11e** would affect the protein levels of these Bcl-2 family members. To verify the involvement of Bcl-2 protein activity in **11e**-induced apoptosis, COLO 205 cells were treated with 50 nM of **11e** for 6, 12, 24, 36, and 48 h. As shown in Fig. 11C, results indicated that **11e** reduced anti-apoptotic Bcl-2 and Bcl-xL levels and increased pro-apoptotic Bax and Bad levels, leading to changes in the Bax/Bcl-2 ratio and the release of cytochrome *c*, which in turn activates cleavage of caspase-9 and activation of caspase-3. These results demonstrate that **11e**-induced cell apoptosis involves the mitochondria-dependent pathway in COLO 205 cells.

*Effects of **11e** on death receptors and expression of their ligands*

Upon binding to their ligands, death receptors trigger apoptosis by stimulating caspase-8 mediated caspase cascades. In this study, expression of several death receptors (Fas,

DR4, and DR5) and their ligands (FasL and TRAIL) were detected in COLO 205 cells (Fig. 12A and B). Compound **11e** treatment induced an increase in DR5, but did not alter Fas levels. These results suggest that DR5 up-regulation plays an important role in **11e**-mediated apoptosis through extrinsic signaling pathways in COLO 205 cells.

***11e**-induced apoptosis is mediated via JNK signaling pathway*

Mitogen-activated protein kinases (MAPK) respond to extracellular stimuli and regulate cellular activities, such as gene expression, mitosis, differentiation, and cell survival/apoptosis. COLO 205 cells were treated with 50 nM of **11e** for 6, 12, 24, 36, and 48 h to investigate the effects of **11e** on extracellular signal-regulated kinases (ERK1/2), JNK and p38 signaling pathways. As shown in Fig. 13, **11e** decreased phospho-ERK1/2, p38, and phospho-p38 expression and induced JNK phosphorylation after 12 h incubation. These observations suggest that JNK activation is involved in **11e**-induced apoptosis.

Discussion and conclusion

In our continuing investigations of 4-phenylquinolin-2(1*H*)-one (4-PQ), new 4-benzyloxyquinolin-2(1*H*)-one derivatives (**7a–e~15a–e**) were designed and synthesized.

In these novel molecules, the 2-quinolone central scaffold of 4-PQ is retained, but the linkage to the 4-phenyl aromatic ring has been extended by the addition of a CH_2O moiety, making a more flexible bridge. Nine compounds (**7e**, **8e**, **9b**, **9c**, **9e**, **10c**, **10e**, **11c** and **11e**) displayed high potency against HL-60, Hep3B, H460, and COLO 205 cells ($IC_{50} < 1$ μM) without affecting normal human Detroit 551 cells ($IC_{50} > 50$ μM). Among them, **11e** exhibited the highest potencies against the above tumor cell lines with IC_{50} values of 0.014, 0.035, 0.04 and 0.028 μM, respectively. Notably, compound **11e** exhibited improved cytotoxicity in comparison with 6,7-methylenedioxy-4-(2,4-dimethoxyphenyl)quinolin-2(1*H*)-one, the most potent 4-PQ analog previously reported (IC_{50} 0.4, 1.0, 0.9, and 7.4 μM against the above four tumor cell lines) (Chen *et al.*, 2013b). SAR study on these new compounds revealed that a 3',5'-dimethoxybenzyloxy moiety, linked at the 4-position of a 6-methoxy-2-quinolone backbone is most favorable for increased antiproliferative activity.

In the NCI-60 assay, compounds **9b**, **9c**, **9e** and **11e** showed broad-spectrum antitumor properties at the nanomolar level. Especially, compound **11e** not only inhibited the growth of numerous cancer cell lines at the low micromolar range, but also exhibited high selectivity against COLO 205 (colon cancer). Furthermore, the preliminary

biological studies indicated that **11e** inhibited cell growth and induced apoptosis in COLO 205 cells. Herein, compound **11e** has been identified as a promising hit and candidate for future development.

Investigation of the anticancer activity of this novel 2-quinolone analog provided data indicating that **11e** exerted highly anti-proliferative activity and cytotoxicity against COLO 205 cells in a dose- and time-dependent manner (Fig. 6C), and resulted in G2/M arrest and apoptosis (Fig. 7A). Microtubules are important cellular targets for anticancer therapy, because of their key role in mitosis (Perez, 2009). Microtubule-targeting agents, including the taxanes, vinca alkaloids, and colchicine, bind to different sites on tubulin and affect stabilization or destabilization of microtubule dynamics (Dumontet *et al.*, 2010). To clarify the molecular regulation of **11e** in G2/M arrest, we first examined its influence on microtubules. Our data showed that **11e** results in the depolymerization of microtubules in COLO 205 cells and disrupts intracellular microtubule networks in intact cells, as shown in the immunofluorescence studies (Fig. 7B). Treatment of **11e** for 24 h resulted in microtubule changes similar to those induced by colchicine. The docked conformation of **11e** was selected as a working model (Fig. 8), based on its similarity to the crystal structure of the bound conformation of DAMA-colchicine in tubulin. The superimposition of **11e** and

DAMA-colchicine based on A-ring showed an extensive overlap of the 2-quinolone cores and C-rings of both molecules had similar orientations. This result supports the hypothesis that the spatial arrangement of the aromatic A- and C-ring plays a crucial role in the activity and binding of compounds that bind to the main binding site of the colchicine domain on α- and β-tubulin. These findings characterize **11e** as a anti-mitotic agent.

Previous investigations have reported that cyclin B1/CDK1 complexes are involved in the regulation of G2/M phase and M-phase transitions (Peters, 2006; Yang *et al.*, 2009). Our data showed increased levels of cyclin B1/CDK1 after **11e** treatment within 6 h to 24 h of treatment (Fig. 9A). These results reveal that treatment with **11e** not only directly contributes to disrupting microtubules in COLO 205 cells, but also induces accumulation of cyclin B1/CDK1. Aurora kinases also play important roles in chromosome alignment, segregation, and cytokinesis during mitosis (Andrews, 2005; Fu *et al.*, 2007; Yang *et al.*, 2007). Our data showed decreased aurora A, phospho-aurora A, aurora B, phospho-aurora B, and phospho-H3 expression after **11e** treatment (Fig. 9B). Therefore, **11e** inhibited the growth of COLO 205 cells and arrested cells at the G2/M phase through the inactivation of aurora kinases.

Apoptosis induced by anti-mitotic agents is widely known to be related to alterations

of cellular signaling pathways (Bhalla, 2003; Jordan *et al.*, 2004). Compound **11e** not only demonstrated broad-spectrum anticancer effects but also produced apoptosis, as shown by the findings of annexin V/PI in COLO 205 cells. Apoptosis regulators have been extensively studied and provide the basis for novel therapeutic strategies aimed at promoting tumor cell death (Lowe *et al.*, 2000; Ghobrial *et al.*, 2005). To investigate the involvement of apoptosis pathways in **11e**-mediated cytotoxicity, we assessed the caspase cascades. The results showed that **11e** induced significant caspase-3, caspase-8, and caspase-9 activities (Fig. 10). Moreover, caspase 8 is one of the regular caspases involved in the extrinsic pathway, while caspase-9 acts in the intrinsic pathway.

The intrinsic pathway is initiated with loss of membrane potential in mitochondria and then the release of cytochrome *c*, AIF, and Endo G from the mitochondria into the cytosol. Cytochrome *c* in conjunction with Apaf-1 and procaspase-9 form an apoptosome. This complex promotes the activation of caspase-9, which in turn activates caspase-3, leading to apoptosis (Green *et al.*, 1998; Dlamini *et al.*, 2004; Eberle *et al.*, 2007). Proteolytic degradation of PARP, a substrate of caspase-3, indicated that caspase activation was involved in **11e**-induced apoptosis in COLO 205 cells (Fig. 10B). To confirm that mitochondria-mediated intrinsic pathways are involved in **11e**-mediated apoptosis, we further monitored the changes of

mitochondrial membrane potential. Our data showed a loss of mitochondrial membrane potential in cells treated with **11e** (Fig. 11A). Fig. 11B shows that **11e** induces a time-dependent effect on cytochrome *c*, AIF, and Endo G translocation from the mitochondria into the cytosol. The Bcl-2 family proteins largely mediate the mitochondrial apoptotic pathway. These proteins include pro-apoptotic members, such as Bax and Bad, which promote mitochondrial permeability, and anti-apoptotic members, such as Bcl-2 and Bcl-xL, which inhibit the pro-apoptotic protein effects or inhibit the mitochondrial release of cytochrome *c* (Antonsson *et al.*, 1997; Bagci *et al.*, 2006). Over-expression of Bcl-2 increases cell survival by suppressing apoptosis. Bax levels increase in conjunction with Bax inhibition of Bcl-2, and the cells undergo apoptosis (Gross *et al.*, 1999; Vela *et al.*, 2013). The present results showed that **11e** treatment resulted in a decrease in the level of anti-apoptotic proteins Bcl-xL and Bcl-2 as well as an increase in the level of pro-apoptotic protein Bax and Bad (Fig. 11C).

The extrinsic pathway is initiated by ligation of transmembrane death receptors (Fas, DR4/5, and TNFR1) with their respective ligands (FasL, TRAIL, and TNFα) triggering the formation of a death-inducing complex to active caspase-8, which in turn cleaves and activates caspase-3 (Ashkenazi *et al.*, 1998; Thorburn, 2004). Enhanced TRAIL expression and stimulation of DR4- and/or DR5-induced apoptosis has been shown in

certain types of cancers, including colon, ovarian, prostate, bladder, and chronic lymphocytic leukemia (O'Flaherty *et al.*, 2006; Lee *et al.*, 2011; Thomas *et al.*, 2013). In the present study, we found that **11e** treatment upregulated the expression of the DR5 protein and influenced the expression of TRAIL (Fig. 12). Caspase-8 is activated by the death receptor. Activated caspase-8 can cleave and activate downstream caspase-3. On the other hand, caspase-8 can induce Bid cleavage. The cleaved Bid causes cytochrome *c* efflux from mitochondria, then activation of caspase-9 and caspase-3. We showed that **11e** induced the cleavage of full-length Bid producing truncated Bid (t-Bid, 17 kDa), which translocated to the mitochondria. These findings together suggest that **11e** induced apoptosis by activating both intrinsic and extrinsic signaling pathways.

Mitogen-activated protein kinases (MAPKs), which belong to a large family of serine-threonine kinase, are critical mediators of the cell membrane to nucleus signal transduction in response to various extracellular stimuli (Pearson *et al.*, 2001; Fang *et al.*, 2005). The three major subfamilies of MAPK include the extracellular-signal-regulated kinases (ERKs), c-Jun N-terminal protein kinase (JNK), and p38. Recent studies have shown that JNKs and p38 pathways are associated with increased apoptosis, whereas the ERK1/2 pathway is shown to suppress apoptosis. In our

experiments, we observed that after 24 h incubation, **11e** increased levels of phosphorylated JNK in COLO 205 cells (Fig. 13). It has been reported that TRAIL can also activate c-Jun N-terminal kinase (JNK) through the adaptor molecules TNF receptor-associated factor 2 (TRAF2) and receptor-interacting protein (RIP) (Lin *et al.*, 2000). It has also been revealed that JNK is activated by TRAIL in colon cancer cells (Mahalingam *et al.*, 2009). In our study, **11e**-activated JNK might play a mediated role in TRAIL-induced COLO 205 cells apoptosis.

In summary, our present study has identified novel 4-benzyloxyquinolin-2(1*H*)-ones as apoptosis inducers. These new series of compounds could be further exploited to obtain analogs with higher activity for cancer chemotherapy. Fig. 14 summarizes the molecular signaling pathways induced by **11e**. We demonstrated that **11e** exhibits broad-spectrum anticancer properties against various solid tumor cells and exerts potential anticancer activity against COLO 205 cells. Based on all mechanistic results, **11e** caused tubulin depolymerization, aurora A and aurora B inactivation, G2/M phase arrest, polyploidy and subsequent apoptosis via both intrinsic and extrinsic apoptotic pathways. These findings suggest that **11e** has potential use as a novel therapeutic agent for the treatment of human colon carcinoma.

Acknowledgments

This investigation was supported by research grants NSC 95-2320-B-039-011-MY3 and NSC 98-2628-B-039-018-MY3 from the National Science Council of the Republic of China awarded to L.-J. Huang, as well as CA177584 from the National Cancer Institute, NIH, awarded to K.-H. Lee. The authors thank the U.S.A. National Cancer Institute (NCI) for screening compounds by the Developmental Therapeutics Program at NCI (Anticancer Screening Program; http://dtp.cancer.gov).

Author Contributions

Conceived and designed the experiments: Y. F. C., L. J. H., K. H. Lee. Performed the experiments: Y. F. C., Y. C. L., C. F. W., T. C. S., H. Y. L., M. H. H. Analyzed the data: Y. F. C., Y. C. L. Wrote the paper: Y. F. C., Y. C. L., S. L. M. N., Y. Z., K. H. L., L. J. H. Submitted compounds to NCI: L. C. C., S. C. K.

Conflict of Interest

The authors declare that there are no conflicts of interest.

References

Abonia R, Insuasty D, Castillo J, Insuasty B, Quiroga J, Nogueras M, *et al.* (2012). Synthesis of novel quinoline-2-one based chalcones of potential anti-tumor activity. *Eur. J. Med. Chem.* 57**:** 29-40.

Ahmed N, Brahmbhatt KG, Singh IP, Bhutani KK (2011). Efficient chemoselective alkylation of quinoline 2,4-diol derivatives in water. *J. Heterocycl. Chem.* 48**:** 237-240.

Ahmed N, Brahmbhatt KG, Sabde S, Mitra D, Singh IP, Bhutani KK (2010). Synthesis and anti-HIV activity of alkylated quinoline 2,4-diols. *Bioorg. Med. Chem.* 18**:** 2872-2879.

Ahvale AB, Prokopcová H, Šefčovičová J, Steinschifter W, Täubl AE, Uray G, *et al.* (2008). 4-Cyano-6,7-dimethoxycarbostyrils with Solvent- and pH-Independent High Fluorescence Quantum Yields and Emission Maxima. *Eur. J. Org. Chem.* 2008**:** 563-571.

Al-Obaid AM, Abdel-Hamide SG, El-Kashef HA, Abdel-Aziz AAM, El-Azab AS, Al-Khamees HA, *et al.* (2009). Substituted quinazolines, part 3. Synthesis, in vitro antitumor activity and molecular modeling study of certain 2-thieno-4(3H)-quinazolinone analogs. *Eur. J. Med. Chem.* 44**:** 2379-2391.

Andrews PD (2005). Aurora kinases: shining lights on the therapeutic horizon? *Oncogene* 24**:** 5005-5015.

Antonsson B, Conti F, Ciavatta A, Montessuit S, Lewis S, Martinou I, *et al.* (1997). Inhibition of Bax channel-forming activity by Bcl-2. *Science* 277**:** 370-372.

Arya K, Agarwal M (2007). Microwave prompted multigram synthesis, structural determination, and photo-antiproliferative activity of fluorinated 4-hydroxyquinolinones. *Bioorg. Med. Chem. Lett.* 17**:** 86-93.

Ashkenazi A, Dixit VM (1998). Death receptors: signaling and modulation. *Science* 281**:** 1305-1308.

Baba A, Kawamura N, Makino H, Ohta Y, Taketomi S, Sohda T (1996). Studies on disease-modifying antirheumatic drugs: synthesis of novel quinoline and quinazoline derivatives and their anti-inflammatory effect. *J. Med. Chem.* 39**:** 5176-5182.

Bagci EZ, Vodovotz Y, Billiar TR, Ermentrout GB, Bahar I (2006). Bistability in apoptosis: roles of bax, bcl-2, and mitochondrial permeability transition pores. *Biophys. J.* 90**:** 1546-1559.

Bhalla KN (2003). Microtubule-targeted anticancer agents and apoptosis. *Oncogene* 22**:** 9075-9086.

Boyd MR, Paull KD (1995). Some practical considerations and applications of the national cancer institute in vitro anticancer drug discovery screen. *Drug Dev. Res.* 34**:** 91-109.

Brunelle JK, Letai A (2009). Control of mitochondrial apoptosis by the Bcl-2 family. *J. Cell. Sci.* 122**:** 437-441.

Buckle DR, Cantello BCC, Smith H, Spicer BA (1975). 4-Hydroxy-3-nitro-2-quinolones and related compounds as inhibitors of allergic reactions. *J. Med. Chem.* 18**:** 726-732.

Cai SX, Zhou Z-L, Huang J-C, Whittemore ER, Egbuwoku ZO, Lü Y, *et al.* (1996). Synthesis and Structure−Activity Relationships of 1,2,3,4-Tetrahydroquinoline-2,3,4-trione 3-Oximes: Novel and Highly Potent Antagonists for NMDA Receptor Glycine Site. *J. Med. Chem.* 39**:** 3248-3255.

Chae M-Y, Swenn K, Kanugula S, Dolan ME, Pegg AE, Moschel RC (1995). 8-Substituted O6-Benzylguanine, Substituted 6(4)-(Benzyloxy)pyrimidine, and Related Derivatives as Inactivators of Human O6-Alkylguanine-DNA Alkyltransferase. *J. Med. Chem.* 38**:** 359-365.

Chan SH, Chui CH, Chan SW, Kok SHL, Chan D, Tsoi MYT, *et al.* (2012). Synthesis of 8-Hydroxyquinoline Derivatives as Novel Antitumor Agents. *ACS Med. Chem. Lett.* 4**:** 170-174.

Chen T-C, Yu D-S, Huang K-F, Fu Y-C, Lee C-C, Chen C-L, *et al.* (2013a). Structure-based design, synthesis and biological evaluation of novel anthra[1,2-d]imidazole-6,11-dione homologues as potential antitumor agents. *Eur. J. Med. Chem.* 69**:** 278-293.

Chen Y-F, Lin Y-C, Huang P-K, Chan H-C, Kuo S-C, Lee K-H, *et al.* (2013b). Design and synthesis of 6,7-methylenedioxy-4-substituted phenylquinolin-2(1H)-one derivatives as novel anticancer agents that induce apoptosis with cell cycle arrest at G2/M phase. *Bioorg. Med. Chem.* 21**:** 5064-5075.

Cheng G, Hao H, Dai M, Liu Z, Yuan Z (2013). Antibacterial action of quinolones: From target to network. *Eur. J. Med. Chem.* 66**:** 555-562.

Chung HS, Woo WS (2001). A quinolone alkaloid with antioxidant activity from the aleurone layer of anthocyanin-pigmented rice. *J. Nat. Prod.* 64**:** 1579-1580.

Coombs TC, Tanega C, Shen M, Wang JL, Auld DS, Gerritz SW, *et al.* (2013). Small-molecule pyrimidine inhibitors of the cdc2-like (Clk) and dual specificity tyrosine phosphorylation-regulated (Dyrk) kinases: Development of chemical probe ML315. *Bioorg. Med. Chem. Lett.* 23**:** 3654-3661.

Cornut D, Lemoine H, Kanishchev O, Okada E, Albrieux F, Beavogui AH, *et al.* (2013). Incorporation of a 3-(2,2,2-trifluoroethyl)-gamma-hydroxy-gamma-lactam motif in the side chain of 4-aminoquinolines. Syntheses and antimalarial activities. *J. Med. Chem.* 56**:** 73-83.

Daniels DS, Mol CD, Arvai AS, Kanugula S, Pegg AE, Tainer JA (2000). Active and alkylated human AGT structures: a novel zinc site, inhibitor and extrahelical base binding. *EMBO J.* 19**:** 1719-1730.

Deng X-Q, Wei C-X, Song M-X, Chai K-Y, Sun Z-G, Quan Z-S (2010). Synthesis and Studies on Anticonvulsant and Antidepressant Activities of 5-Alkoxy-tetrazolo[1,5-a]quinolines. *Bull. Korean Chem. Soc.* 31**:** 447-452.

Dlamini Z, Mbita Z, Zungu M (2004). Genealogy, expression, and molecular mechanisms in apoptosis. *Pharmacol. Ther.* 101**:** 1-15.

Dolan ME, Pegg AE (1997). O6-benzylguanine and its role in chemotherapy. *Clin. Cancer Res.* 3**:** 837-847.

Doležal K, Popa I, Kryštof V, Spíchal L, Fojtíková M, Holub J, *et al.* (2006). Preparation and biological activity of 6-benzylaminopurine derivatives in plants and human cancer cells. *Bioorg. Med. Chem.* 14**:** 875-884.

Dumontet C, Jordan MA (2010). Microtubule-binding agents: a dynamic field of cancer therapeutics. *Nat. Rev. Drug Discov.* 9**:** 790-803.

Eberle J, Fecker LF, Forschner T, Ulrich C, Rowert-Huber J, Stockfleth E (2007). Apoptosis pathways as promising targets for skin cancer therapy. *Br. J. Dermatol.* 156 Suppl 3**:** 18-24.

Elmore S (2007). Apoptosis: a review of programmed cell death. *Toxicol. Pathol.* 35**:** 495-516.

Fang JY, Richardson BC (2005). The MAPK signalling pathways and colorectal cancer. *Lancet Oncol.* 6**:** 322-327.

Fesik SW (2005). Promoting apoptosis as a strategy for cancer drug discovery. *Nat. Rev. Cancer* 5**:** 876-885.

Fiorito J, Saeed F, Zhang H, Staniszewski A, Feng Y, Francis YI, *et al.* (2013). Synthesis of quinoline derivatives: Discovery of a potent and selective phosphodiesterase 5 inhibitor for the treatment of Alzheimer's disease. *Eur. J. Med. Chem.* 60**:** 285-294.

Fischer U, Schulze-Osthoff K (2005). Apoptosis-based therapies and drug targets. *Cell Death Differ.* 12**:** 942-961.

Folger O, Jerby L, Frezza C, Gottlieb E, Ruppin E, Shlomi T (2011). Predicting selective drug targets in cancer through metabolic networks. *Mol. Syst. Biol.* 7**:** 501.

Font M, González Á, Palop JA, Sanmartín C (2011). New insights into the structural requirements for pro-apoptotic agents based on 2,4-diaminoquinazoline, 2,4-

diaminopyrido[2,3-d]pyrimidine and 2,4-diaminopyrimidine derivatives. *Eur. J. Med. Chem.* 46**:** 3887-3899.

Freeman GA, Andrews Iii CW, 3rd, Hopkins AL, Lowell GS, Schaller LT, Cowan JR, *et al.* (2004). Design of non-nucleoside inhibitors of HIV-1 reverse transcriptase with improved drug resistance properties. 2. *J. Med. Chem.* 47**:** 5923-5936.

Fu J, Bian M, Jiang Q, Zhang C (2007). Roles of Aurora Kinases in Mitosis and Tumorigenesis. *Mol. Cancer Res.* 5**:** 1-10.

Ghobrial IM, Witzig TE, Adjei AA (2005). Targeting apoptosis pathways in cancer therapy. *CA Cancer J. Clin.* 55**:** 178-194.

Gibson AE, Arris CE, Bentley J, Boyle FT, Curtin NJ, Davies TG, *et al.* (2002). Probing the ATP ribose-binding domain of cyclin-dependent kinases 1 and 2 with O(6)-substituted guanine derivatives. *J. Med. Chem.* 45**:** 3381-3393.

Green DR, Reed JC (1998). Mitochondria and Apoptosis. *Science* 281**:** 1309-1312.

Gross A, McDonnell JM, Korsmeyer SJ (1999). BCL-2 family members and the mitochondria in apoptosis. *Genes Dev.* 13**:** 1899-1911.

Guo L-J, Wei C-X, Jia J-H, Zhao L-M, Quan Z-S (2009). Design and synthesis of 5-alkoxy-[1,2,4]triazolo[4,3-a]quinoline derivatives with anticonvulsant activity. *Eur. J. Med. Chem.* 44**:** 954-958.

He J, Lion U, Sattler I, Gollmick FA, Grabley S, Cai J, *et al.* (2005). Diastereomeric Quinolinone Alkaloids from the Marine-Derived Fungus Penicillium janczewskii. *J. Nat. Prod.* 68**:** 1397-1399.

Holbeck SL (2004). Update on NCI in vitro drug screen utilities. *Eur. J. Cancer* 40**:** 785-793.

Holbeck SL, Collins JM, Doroshow JH (2010). Analysis of Food and Drug Administration–Approved Anticancer Agents in the NCI60 Panel of Human Tumor Cell Lines. *Mol. Cancer Ther.* 9**:** 1451-1460.

Hopkins AL, Ren J, Milton J, Hazen RJ, Chan JH, Stuart DI, *et al.* (2004). Design of Non-Nucleoside Inhibitors of HIV-1 Reverse Transcriptase with Improved Drug Resistance Properties. 1. *J. Med. Chem.* 47**:** 5912-5922.

Ito C, Itoigawa M, Furukawa A, Hirano T, Murata T, Kaneda N, *et al.* (2004). Quinolone Alkaloids with Nitric Oxide Production Inhibitory Activity from Orixa japonica. *J. Nat. Prod.* 67**:** 1800-1803.

Jorda R, Havlicek L, McNae IW, Walkinshaw MD, Voller J, Sturc A, *et al.* (2011). Pyrazolo[4,3-d]pyrimidine bioisostere of roscovitine: evaluation of a novel selective inhibitor of cyclin-dependent kinases with antiproliferative activity. *J. Med. Chem.* 54**:** 2980-2993.

Jordan MA, Wilson L (2004). Microtubules as a target for anticancer drugs. *Nat. Rev. Cancer* 4**:** 253-265.

Kappe T, Karem AS, Stadlbauer W (1988). Synthesis of benzo-halogenated 4-hydroxy-2(1H)-quinolones. *J. Heterocycl. Chem.* 25**:** 857-862.

Kaufmann SH, Earnshaw WC (2000). Induction of Apoptosis by Cancer Chemotherapy. *Exp. Cell Res.* 256**:** 42-49.

Keen N, Taylor S (2004). Aurora-kinase inhibitors as anticancer agents. *Nat. Rev. Cancer* 4**:** 927-936.

LaPlante SR, Bilodeau F, Aubry N, Gillard JR, O'Meara J, Coulombe R (2013). N-versus O-alkylation: Utilizing NMR methods to establish reliable primary structure determinations for drug discovery. *Bioorg. Med. Chem. Lett.* 23**:** 4663-4668.

Lee J-C, Chou L-C, Huang C-H, Chung J-G, Huang L-J, Lee K-H, *et al.* (2011). CHM-1 induces apoptosis via p38-mediated upregulation of DR5 expression in human ovarian cancer SKOV3 cells. *Eur. J. Pharmacol.* 670**:** 96-104.

Lewis FD, Reddy GD, Elbert JE, Tillberg BE, Meltzer JA, Kojima M (1991). Lewis acid catalysis of photochemical reactions. 10. Spectroscopy and photochemistry of 2-

quinolones and their Lewis acid complexes. *J. Org. Chem.* 56**:** 5311-5318.

Lilienkampf A, Mao J, Wan B, Wang Y, Franzblau SG, Kozikowski AP (2009). Structure-activity relationships for a series of quinoline-based compounds active against replicating and nonreplicating Mycobacterium tuberculosis. *J. Med. Chem.* 52**:** 2109-2118.

Lin Y, Devin A, Cook A, Keane MM, Kelliher M, Lipkowitz S, *et al.* (2000). The Death Domain Kinase RIP Is Essential for TRAIL (Apo2L)-Induced Activation of IκB Kinase and c-Jun N-Terminal Kinase. *Mol. Cell. Biol.* 20**:** 6638-6645.

Liu J, Grimison B, Maller JL (2007). New insight into metaphase arrest by cytostatic factor: from establishment to release. *Oncogene* 26**:** 1286-1289.

Longley DB, Harkin DP, Johnston PG (2003). 5-Fluorouracil: mechanisms of action and clinical strategies. *Nat. Rev. Cancer* 3**:** 330-338.

Lowe SW, Lin AW (2000). Apoptosis in cancer. *Carcinogenesis* 21**:** 485-495.

Mahalingam D, Keane M, Pirianov G, Mehmet H, Samali A, Szegezdi E (2009). Differential activation of JNK1 isoforms by TRAIL receptors modulate apoptosis of colon cancer cell lines. *Br. J. Cancer* 100**:** 1415-1424.

MOHAMED EHA (1991). One-step synthesis of 4-hydroxycarbostyrils .6. *J. Chem. Soc. Pak.* 13**:** 166-168.

Moradi-e-Rufchahi EOl (2010). Synthesis of 6-chloro and 6-fluoro-4-hydroxyl-2-quinolone and their azo disperse dyes. *Chin. Chem. Lett.* 21**:** 542-546.

Mosmann T (1983). Rapid colorimetric assay for cellular growth and survival: Application to proliferation and cytotoxicity assays. *J. Immunol. Methods.* 65**:** 55-63.

Mott BT, Tanega C, Shen M, Maloney DJ, Shinn P, Leister W, *et al.* (2009). Evaluation of substituted 6-arylquinazolin-4-amines as potent and selective inhibitors of cdc2-like kinases (Clk). *Bioorg. Med. Chem. Lett.* 19**:** 6700-6705.

Mukherjee S, Pal M (2013). Quinolines: a new hope against inflammation. *Drug Discov. Today* 18**:** 389-398.

Nadaraj V, Selvi ST, Sasi R (2006). Microwave-assisted synthesis of quinoline alkaloids: 4-Methoxy-1-methyl-2-quinolinone and its analogs. *ARKIVOC* x**:** 82-89.

Nakashima K-i, Oyama M, Ito T, Akao Y, Witono JR, Darnaedi D, *et al.* (2012). Novel quinolinone alkaloids bearing a lignoid moiety and related constituents in the leaves of Melicope denhamii. *Tetrahedron* 68**:** 2421-2428.

Noolvi MN, Patel HM, Kamboj S, Kaur A, Mann V (2012). 2,6-Disubstituted imidazo[2,1-b][1,3,4]thiadiazoles: Search for anticancer agents. *Eur. J. Med. Chem.* 56**:** 56-69.

O'Flaherty J, Mei Y, Freer M, Weyman CM (2006). Signaling through the TRAIL receptor DR5/FADD pathway plays a role in the apoptosis associated with skeletal myoblast differentiation. *Apoptosis* 11**:** 2103-2113.

Oh S, Park SB (2011). A design strategy for drug-like polyheterocycles with privileged substructures for discovery of specific small-molecule modulators. *Chem. Commun.* 47**:** 12754-12761.

Pandey S, Agarwal P, Srivastava K, RajaKumar S, Puri SK, Verma P, *et al.* (2013). Synthesis and bioevaluation of novel 4-aminoquinoline-tetrazole derivatives as potent antimalarial agents. *Eur. J. Med. Chem.* 66**:** 69-81.

Park KK, Lee JJ (2004). Facile synthesis of 4-phenylquinolin-2(1H)-one derivatives from N-acyl-o-aminobenzophenones. *Tetrahedron* 60**:** 2993-2999.

Park S-J, Lee J-C, Lee K-I (2007). A Facile Synthesis of 4-Hydroxycoumarin and 4-Hydroxy-2-quinolone Derivatives. *Bull. Korean Chem. Soc.* 28**:** 1203-1205.

Paruch K, Dwyer MP, Alvarez C, Brown C, Chan T-Y, Doll RJ, *et al.* (2007). Pyrazolo[1,5-a]pyrimidines as orally available inhibitors of cyclin-dependent kinase 2. *Bioorg. Med. Chem. Lett.* 17**:** 6220-6223.

Pearson G, Robinson F, Beers Gibson T, Xu BE, Karandikar M, Berman K, *et al.* (2001). Mitogen-activated protein (MAP) kinase pathways: regulation and physiological functions. *Endocr. Rev.* 22**:** 153-183.

Perez EA (2009). Microtubule inhibitors: Differentiating tubulin-inhibiting agents based on mechanisms of action, clinical activity, and resistance. *Mol. Cancer Ther.* 8**:** 2086-2095.

Peters J-M (2006). The anaphase promoting complex/cyclosome: a machine designed to destroy. *Nat. Rev. Mol. Cell Biol.* 7**:** 644-656.

Pirrung MC, Blume F (1999). Rhodium-Mediated Dipolar Cycloaddition of Diazoquinolinediones. *J. Org. Chem.* 64**:** 3642-3649.

Priya N, Gupta A, Chand K, Singh P, Kathuria A, Raj HG, *et al.* (2010). Characterization of 4-methyl-2-oxo-1,2-dihydroquinolin-6-yl acetate as an effective antiplatelet agent. *Bioorg. Med. Chem.* 18**:** 4085-4094.

Rastogi T, Hildesheim A, Sinha R (2004). Opportunities for cancer epidemiology in developing countries. *Nat. Rev. Cancer* 4**:** 909-917.

Ravelli RBG, Gigant B, Curmi PA, Jourdain I, Lachkar S, Sobel A, *et al.* (2004). Insight into tubulin regulation from a complex with colchicine and a stathmin-like domain. *Nature* 428**:** 198-202.

Roy MJ, Vom A, Czabotar PE, Lessene G (2014). Cell death and the mitochondria: therapeutic targeting of the BCL-2 family-driven pathway. *Br. J. Pharmacol.* 171**:** 1973-1987.

Ruiz FM, Gil-Redondo Rn, Morreale A, Ortiz AnR, Fábrega C, Bravo Jn (2008). Structure-Based Discovery of Novel Non-nucleosidic DNA Alkyltransferase Inhibitors: Virtual Screening and in Vitro and in Vivo Activities. *J. Chem. Inf. Model.* 48**:** 844-854.

Shoemaker RH (2006). The NCI60 human tumour cell line anticancer drug screen. *Nat. Rev. Cancer* 6**:** 813-823.

Solomon VR, Lee H (2011). Quinoline as a privileged scaffold in cancer drug discovery. *Curr. Med. Chem.* 18**:** 1488-1508.

Terashima I, Kohda K (1998). Inhibition of Human O6-Alkylguanine-DNA Alkyltransferase and Potentiation of the Cytotoxicity of Chloroethylnitrosourea by 4(6)-(Benzyloxy)-2,6(4)-diamino-5-(nitro or nitroso)pyrimidine Derivatives and Analogues. *J. Med. Chem.* 41**:** 503-508.

Thomas S, Vasudevan S, Thamkachy R, Lekshmi S, Santhoshkumar T, Rajasekharan K, *et al.* (2013). Upregulation of DR5 receptor by the diaminothiazole DAT1 [4-amino-5-benzoyl-2-(4-methoxy phenyl amino) thiazole] triggers an independent extrinsic pathway of apoptosis in colon cancer cells with compromised pro and antiapoptotic proteins. *Apoptosis* 18**:** 713-726.

Thorburn A (2004). Death receptor-induced cell killing. *Cell. Signal.* 16**:** 139-144.

Trott O, Olson AJ (2010). AutoDock Vina: Improving the speed and accuracy of docking with a new scoring function, efficient optimization, and multithreading. *J. Comput. Chem.* 31**:** 455-461.

van Engeland M, Nieland LJ, Ramaekers FC, Schutte B, Reutelingsperger CP (1998). Annexin V-affinity assay: a review on an apoptosis detection system based on phosphatidylserine exposure. *Cytometry* 31**:** 1-9.

Vela L, Gonzalo O, Naval J, Marzo I (2013). Direct Interaction of Bax and Bak Proteins with Bcl-2 Homology Domain 3 (BH3)-only Proteins in Living Cells Revealed by Fluorescence Complementation. *J. Biol. Chem.* 288**:** 4935-4946.

Wang Y, Ai J, Chen Y, Wang L, Liu G, Geng M, *et al.* (2011). Synthesis and c-Met kinase inhibition of 3,5-disubstituted and 3,5,7-trisubstituted quinolines: identification of 3-(4-acetylpiperazin-1-yl)-5-(3-nitrobenzylamino)-7- (trifluoromethyl)quinoline as a novel anticancer agent. *J. Med. Chem.* 54**:** 2127-2142.

Yang J-S, Chen G-W, Hsia T-C, Ho H-C, Ho C-C, Lin M-W, *et al.* (2009). Diallyl disulfide induces apoptosis in human colon cancer cell line (COLO 205) through the induction of reactive oxygen species, endoplasmic reticulum stress, caspases casade

and mitochondrial-dependent pathways. *Food Chem. Toxicol.* 47**:** 171-179.

Yang J, Ikezoe T, Nishioka C, Tasaka T, Taniguchi A, Kuwayama Y, *et al.* (2007). AZD1152, a novel and selective aurora B kinase inhibitor, induces growth arrest, apoptosis, and sensitization for tubulin depolymerizing agent or topoisomerase II inhibitor in human acute leukemia cells in vitro and in vivo. *Blood* 110**:** 2034-2040.

Zatloukal M, Jorda R, Gucký T, Řezníčková E, Voller J, Pospíšil T, *et al.* (2013). Synthesis and in vitro biological evaluation of 2,6,9-trisubstituted purines targeting multiple cyclin-dependent kinases. *Eur. J. Med. Chem.* 61**:** 61-72.

Zhai D, Jin C, Huang Z, Satterthwait AC, Reed JC (2008). Differential Regulation of Bax and Bak by Anti-apoptotic Bcl-2 Family Proteins Bcl-B and Mcl-1. *J. Biol. Chem.* 283**:** 9580-9586.

Zhang S-L, Huang Z-S, Li Y-M, Chan ASC, Gu L-Q (2008). Synthesis of zwitterionic 4-hydroxy-2(1H)-quinolinone derivatives. *Tetrahedron* 64**:** 4403-4407.

Zhang Y, Fang Y, Liang H, Wang H, Hu K, Liu X, *et al.* (2013). Synthesis and antioxidant activities of 2-oxo-quinoline-3-carbaldehyde Schiff-base derivatives. *Bioorg. Med. Chem. Lett.* 23**:** 107-111.

Zhu R, Baumann RP, Penketh PG, Shyam K, Sartorelli AC (2013). Hypoxia-Selective O6-Alkylguanine-DNA Alkyltransferase Inhibitors: Design, Synthesis, and Evaluation of 6-(Benzyloxy)-2-(aryldiazenyl)-9H-purines as Prodrugs of O6-Benzylguanine. *J. Med. Chem.* 56**:** 1355-1359.

Zhuang S-H, Lin Y-C, Chou L-C, Hsu M-H, Lin H-Y, Huang C-H, *et al.* (2013). Synthesis and anticancer activity of 2,4-disubstituted furo[3,2-b]indole derivatives. *Eur. J. Med. Chem.* 66**:** 466-479.

Supporting information

Supporting information includes physical and spectroscopic information, NMR, mass,

and IR spectra of synthetic target compounds, as well as detailed NCI-60 results for compounds **9b**, **9c**, **9e**, and **11e**.

Figures and Legends

Fig. 1. The structures of some anticancer agents and the general structure of the target compounds (**7a–e~15a–e**).

Fig. 2. Alkylation of 4-hydroxyquinolin-2(1*H*)-ones. (A) Tautomerism of 4-hydroxyquinolin-2(1*H*)-one derivatives. (B) Key HMBC correlations (blue arrows) of **11e** indicated alkylation at the 4-OH position.

Fig. 3. Subpanel tumor cell lines selectivity ratios of selected compounds **9b**, **9c**, **9e**, and **11e**.

Fig. 4. Dose-response curves of compound **11e** against colon cancer cell lines.

Fig. 5. Compound **11e** induced time-dependent apoptosis in COLO 205 cells. COLO 205 cells were treated with 50 nM of **11e** for 0, 12, 24, 36, and 48 h. (A) Compound **11e** induced morphological changes in COLO 205 cells. (B) Fluorescent images of Hoechst staining showing **11e** induced cell death. The black arrowhead indicates an apoptotic nucleus, and the white arrowheads indicate multinucleate cells. (C) Confirmation of **11e**-induced apoptosis was assessed using annexin V/PI staining and flow cytometry. The fraction of annexin V-positive COLO 205 cells was 5.5% prior to treatment and 7.6%, 12.7%, 20.9%, and 21.8% after treatment with **11e** for 12 h, 24 h, 36 h, and 48 h, respectively. Scale bar = 20 μm.

Fig. 6. Effects of **11e** on the cytotoxicity of COLO 205 cells. (A) Chemical structure of **11e**. (B) COLO 205 cells were exposed to different concentrations of **11e** for 48 h. (C) COLO 205 cells were exposed to 0 nM, 10 nM, 25 nM, 50 nM, 75 nM, and 100 nM **11e** for 24 h, 48 h, and 72 h. Cell viability was assessed using the MTT assay. The data are presented as mean ± SEM of three independent experiments. Cells without treatment

served as a control. * $p<0.001$ vs. control.

Fig. 7. 11e delays M-phase progression and caused microtubule disassembly in cultured cells. (A) Flow cytometry analysis of cell cycle distribution in COLO 205 colon cancer cell line treated with 50 nM of **11e** for 0 h, 6 h, 12 h, 24 h, 36 h, and 48 h. (B) The effect of **11e** on the microtubule formation in COLO 205 cells. Cells were incubated with 0.1 % DMSO, 50 nM **11e**, 1 μM colchicine, or 1 μM taxol for 24 h. Immunofluorescence for α-tubulin (green) and PI nuclear staining (red). Cells were visualized using confocal microscopy.

Fig. 8. The docked binding mode of **11e** is shown with the binding site of tubulin (PDB entry 1SA0). The figures were performed using PyMol. (A) The binding mode of DAMA-colchicine (red stick model) and tubulin. (B) The binding mode of **11e** (yellow stick model) and tubulin. (C) DAMA-colchicine and **11e** occupy similar binding space in tubulin (shown as surface of tubulin cavity). (D) The superimposition of DAMA-colchicine and **11e**.

Fig. 9. Compound **11e** increased G2/M phase checkpoint protein expression. COLO 205 cells were treated with 50 nM **11e** for the indicated time periods and lysed for protein extraction. Protein samples (40 μg protein/lane) were separated using 10% SDS-PAGE and subjected to immunoblotting with antibodies specific to cyclin B1, CDK1, phospho-CDK1 (A), aurora A, phospho-aurora A, aurora B, phospho-aurora B, H3, phospho-H3 (B), and β-actin (n = 3 independent experiments). β-Actin was used as a loading control.

Fig. 10. Compound **11e** induced caspase-3, caspase-8, and caspase-9 activity in COLO 205 cells. COLO 205 cells were treated with 50 nM **11e** for the indicated times and lysed for protein extraction. Protein samples (40 μg protein/lane) were separated using 10% SDS-PAGE and subjected to immunoblotting with antibodies specific to caspase-9,

caspase-8, caspase-3, PARP, and β-actin (n = 3 independent experiments). β-Actin was used as a loading control.

Fig. 11. Compound **11e** induced mitochondrial apoptosis pathway in COLO 205 cells. (A) Effects of **11e** on mitochondrial membrane potential in COLO 205 cells. Cells (1×10^6 cells/ml) were untreated or treated with **11e** (50 nM, 6-48 h) to induce apoptosis. Cells were stained with JC-1 according to the protocol on a BD™ MitoScreen as described in the section Methods for Staining Cells with JC-1 and Analyzing by Flow Cytometry. (B) COLO 205 cells were treated with 50 nM **11e** for the indicated times and lysed for protein extraction. Protein samples (40 μg protein/lane) were separated using 10% SDS-PAGE and subjected to immunoblotting with antibodies specific to AIF, Endo G, Apaf-1, cytochrome *c*, and β-actin (n = 3 independent experiments). (C) Compound **11e** affected Bcl-2 family proteins in COLO 205 cells. COLO 205 cells were treated with 50 nM **11e** for the indicated times and lysed for protein extraction. Protein samples (40 μg protein/lane) were separated using 10% SDS-PAGE and subjected to immunoblotting with antibodies specific to Bid, Bax, Bad, Bcl-xL, Bcl-2, and β-actin (n = 3 independent experiments). β-Actin was used as a loading control.

Fig. 12. Compound **11e** induced death receptor apoptosis pathway in COLO 205 cells. COLO 205 cells were treated with 50 nM **11e** for the indicated times and lysed for protein extraction. Protein samples (40 μg protein/lane) were separated using 10% SDS-PAGE and subjected to immunoblotting with antibodies specific to Fas, TNFR1, DR4, DR5 (A), FasL, TNF-α, TRAIL (B), and β-actin (n = 3 independent experiments). β-Actin was used as a loading control.

Fig. 13. Expression of MAPKs in the **11e-**treated COLO 205 cells. COLO 205 cells were treated with 50 nM **11e** for the indicated times and lysed for protein extraction. Protein

samples (40 μg protein/lane) were separated using 10% SDS-PAGE and subjected to immunoblotting with antibodies specific to ERK1/2, phospho-ERK1/2, JNK, phospho-JNK, p38, phospho-p38 and β-actin (n = 3 independent experiments). β-Actin was used as a loading control.

Fig. 14. The signaling pathways of **11e**-induced G2/M phase arrest and apoptosis in human colon cancer COLO 205 cells.

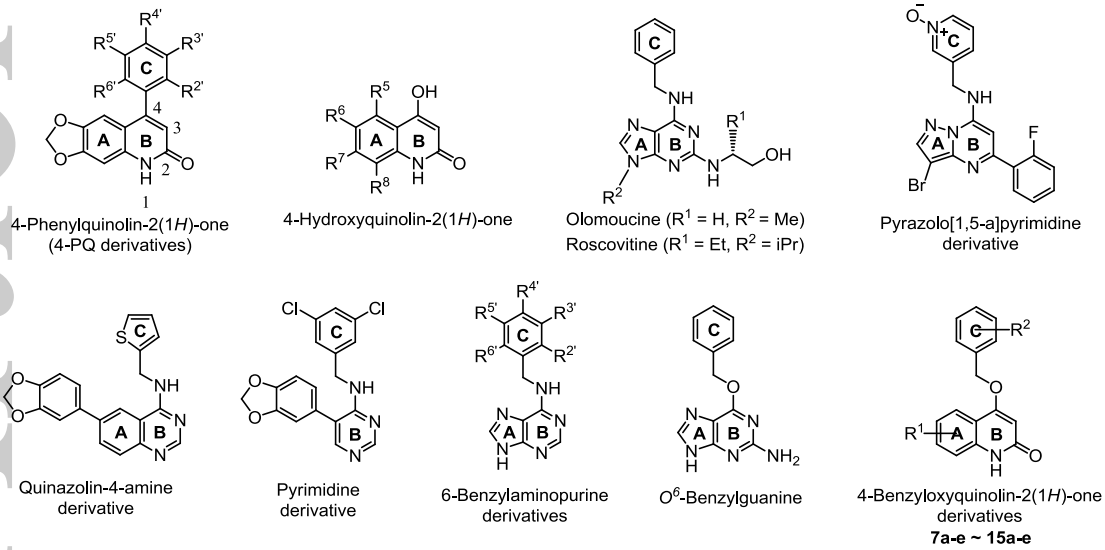

Fig. 1. The structures of some anticancer agents and the general structure of the target compounds (**7a–e~15a–e**).

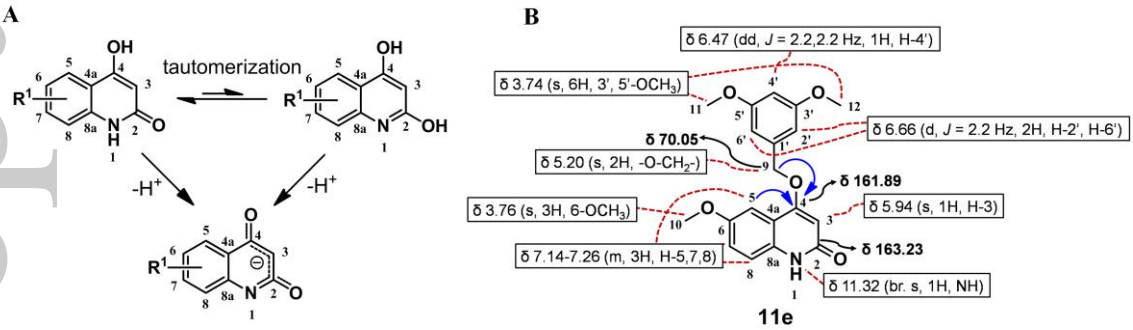

Fig. 2. Alkylation of 4-hydroxyquinolin-2(1*H*)-ones. (A) Tautomerism of 4-hydroxyquinolin-2(1*H*)-one derivatives. (B) Key HMBC correlations (blue arrows) of **11e** indicated alkylation at the 4-OH position.

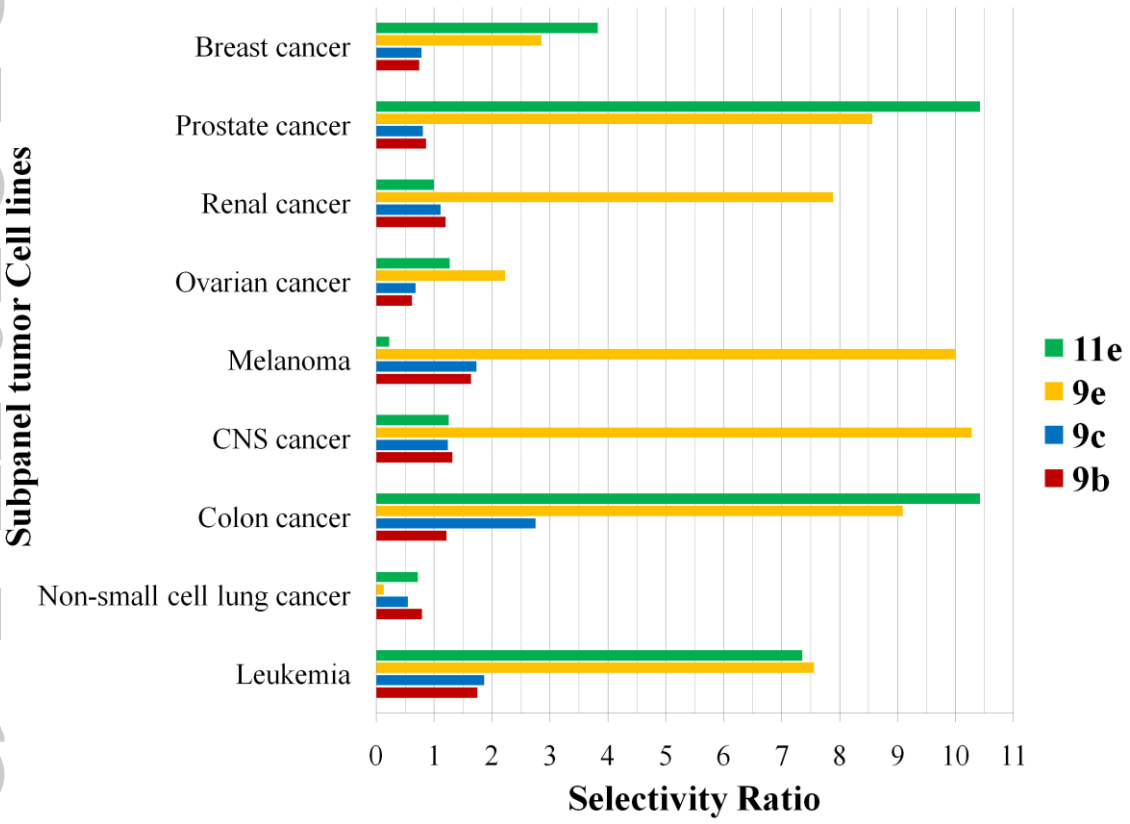

Fig. 3. Subpanel tumor cell lines selectivity ratios of selected compounds **9b**, **9c**, **9e**, and **11e**.

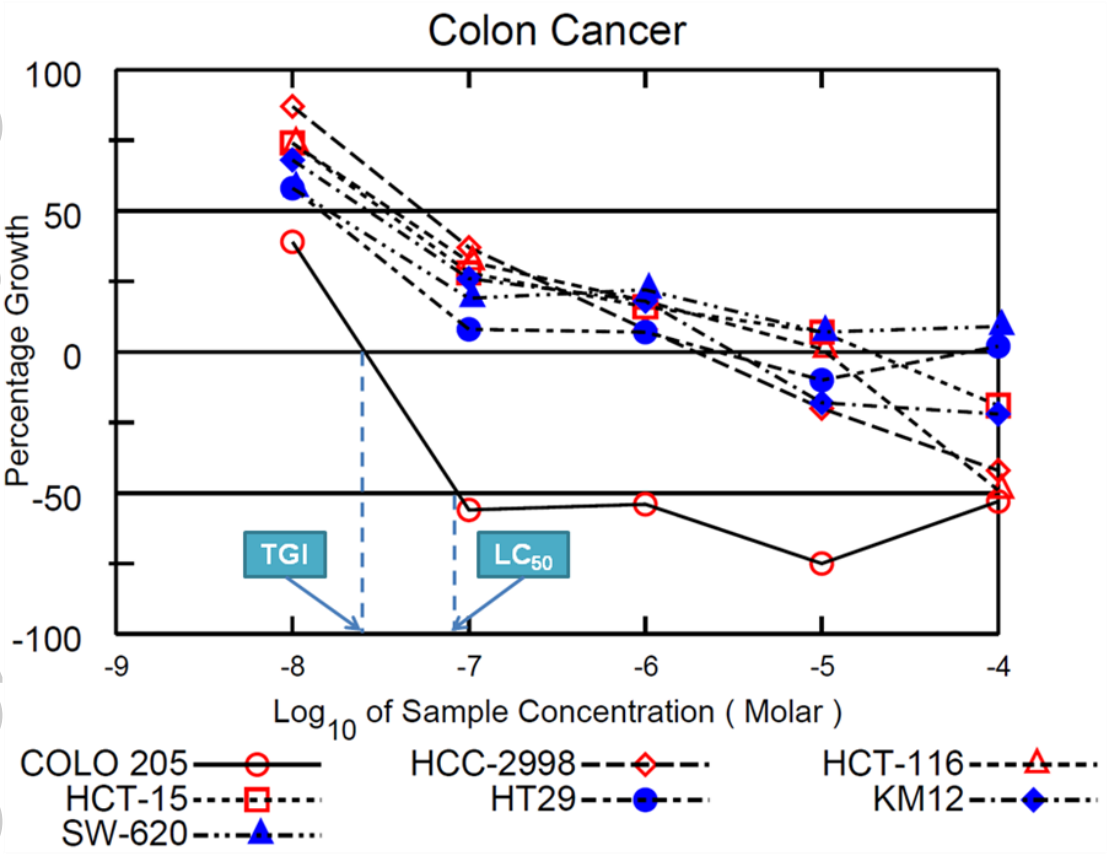

Fig. 4. Dose-response curves of compound **11e** against colon cancer cell lines.

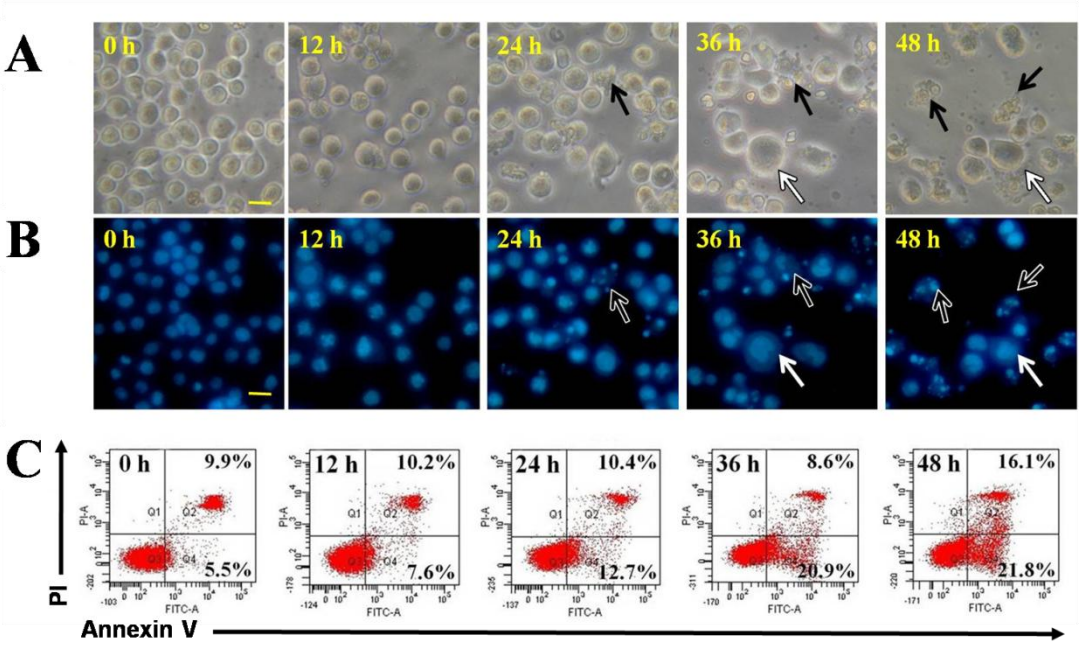

Fig. 5. Compound **11e** induced time-dependent apoptosis in COLO 205 cells. COLO 205 cells were treated with 50 nM of **11e** for 0, 12, 24, 36, and 48 h. (A) Compound **11e** induced morphological changes in COLO 205 cells. (B) Fluorescent images of Hoechst staining showing **11e** induced cell death. The black arrowhead indicates an apoptotic nucleus, and the white arrowheads indicate multinucleate cells. (C) Confirmation of **11e**-induced apoptosis was assessed using annexin V/PI staining and flow cytometry. The fraction of annexin V-positive COLO 205 cells was 5.5% prior to treatment and 7.6%, 12.7%, 20.9%, and 21.8% after treatment with **11e** for 12 h, 24 h, 36 h, and 48 h, respectively. Scale bar = 20 μm.

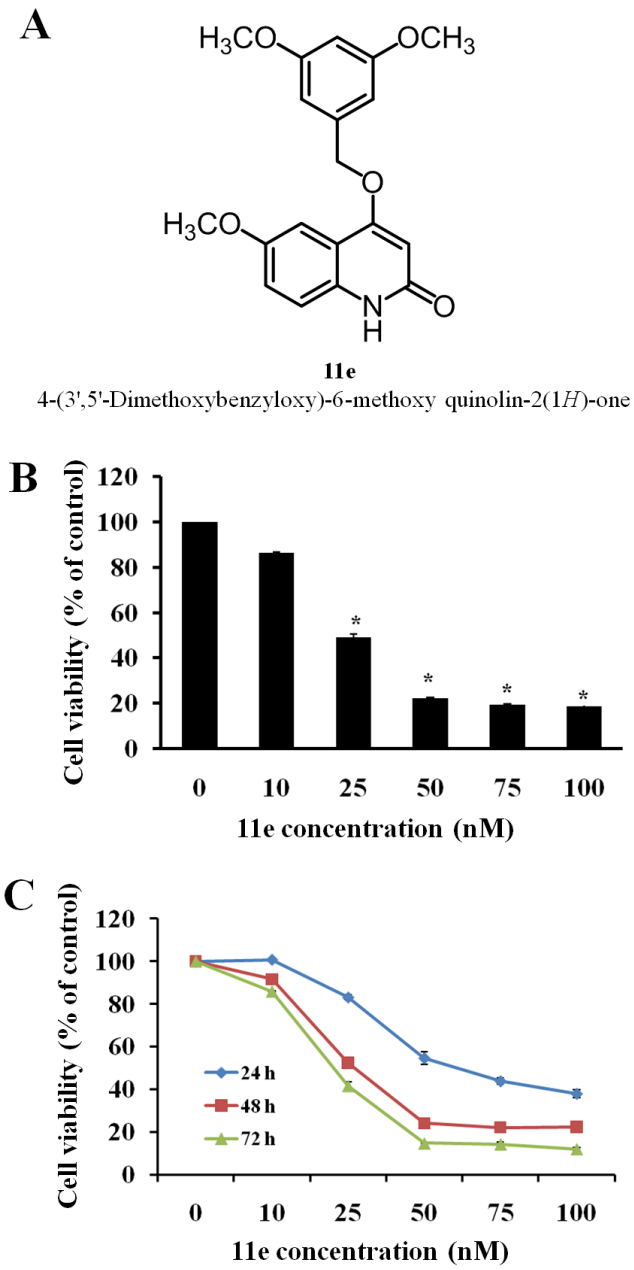

Fig. 6. Effects of **11e** on the cytotoxicity of COLO 205 cells. (A) Chemical structure of **11e**. (B) COLO 205 cells were exposed to different concentrations of **11e** for 48 h. (C) COLO 205 cells were exposed to 0 nM, 10 nM, 25 nM, 50 nM, 75 nM, and 100 nM **11e** for 24 h, 48 h, and 72 h. Cell viability was assessed using the MTT assay. The data are presented as mean ± SEM of three independent experiments. Cells without treatment served as a control. * p<0.001 vs. control.

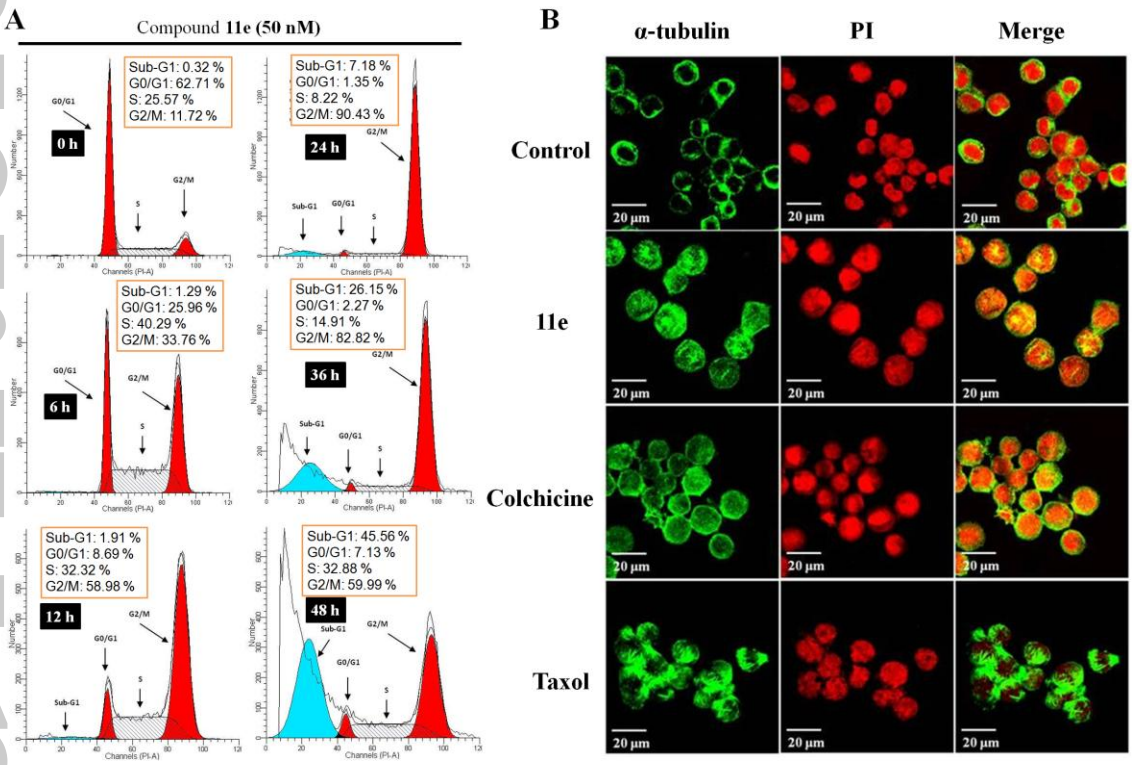

Fig. 7. 11e delays M-phase progression and caused microtubule disassembly in cultured cells. (A) Flow cytometry analysis of cell cycle distribution in COLO 205 colon cancer cell line treated with 50 nM of **11e** for 0 h, 6 h, 12 h, 24 h, 36 h, and 48 h. (B) The effect of **11e** on the microtubule formation in COLO 205 cells. Cells were incubated with 0.1 % DMSO, 50 nM **11e**, 1 μM colchicine, or 1 μM taxol for 24 h. Immunofluorescence for α-tubulin (green) and PI nuclear staining (red). Cells were visualized using confocal microscopy.

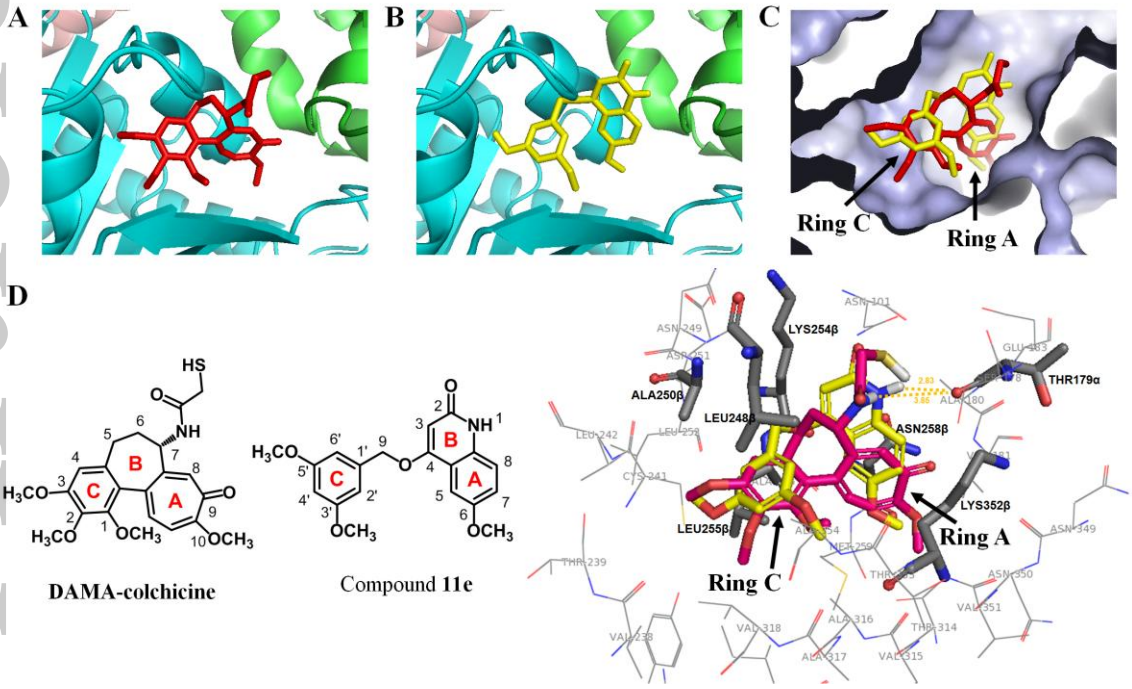

Fig. 8. The docked binding mode of **11e** is shown with the binding site of tubulin (PDB entry 1SA0). The figures were performed using PyMol. (A) The binding mode of DAMA-colchicine (red stick model) and tubulin. (B) The binding mode of **11e** (yellow stick model) and tubulin. (C) DAMA-colchicine and **11e** occupy similar binding space in tubulin (shown as surface of tubulin cavity). (D) The superimposition of DAMA-colchicine and **11e**.

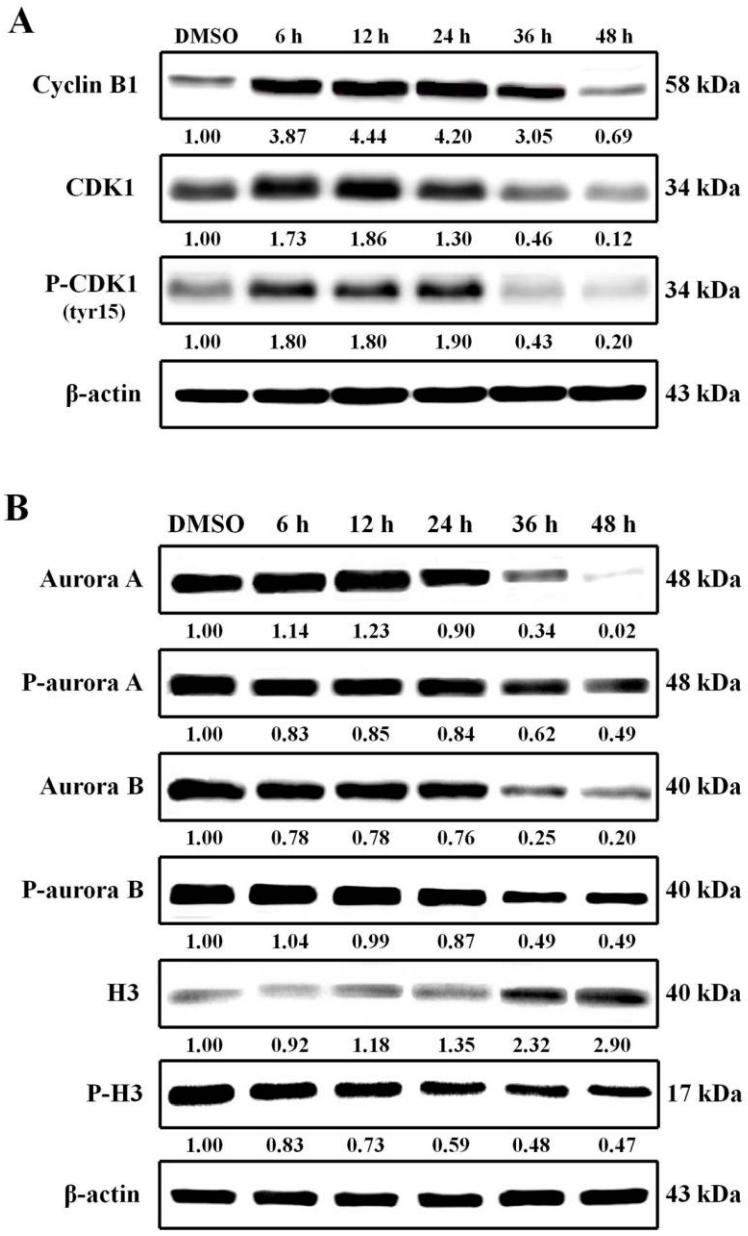

Fig. 9. Compound **11e** increased G2/M phase checkpoint protein expression. COLO 205 cells were treated with 50 nM **11e** for the indicated time periods and lysed for protein extraction. Protein samples (40 μg protein/lane) were separated using 10% SDS-PAGE and subjected to immunoblotting with antibodies specific to cyclin B1, CDK1, phospho-CDK1 (A), aurora A, phospho-aurora A, aurora B, phospho-aurora B, H3, phospho-H3 (B), and β-actin (n = 3 independent experiments). β-Actin was used as a loading control.

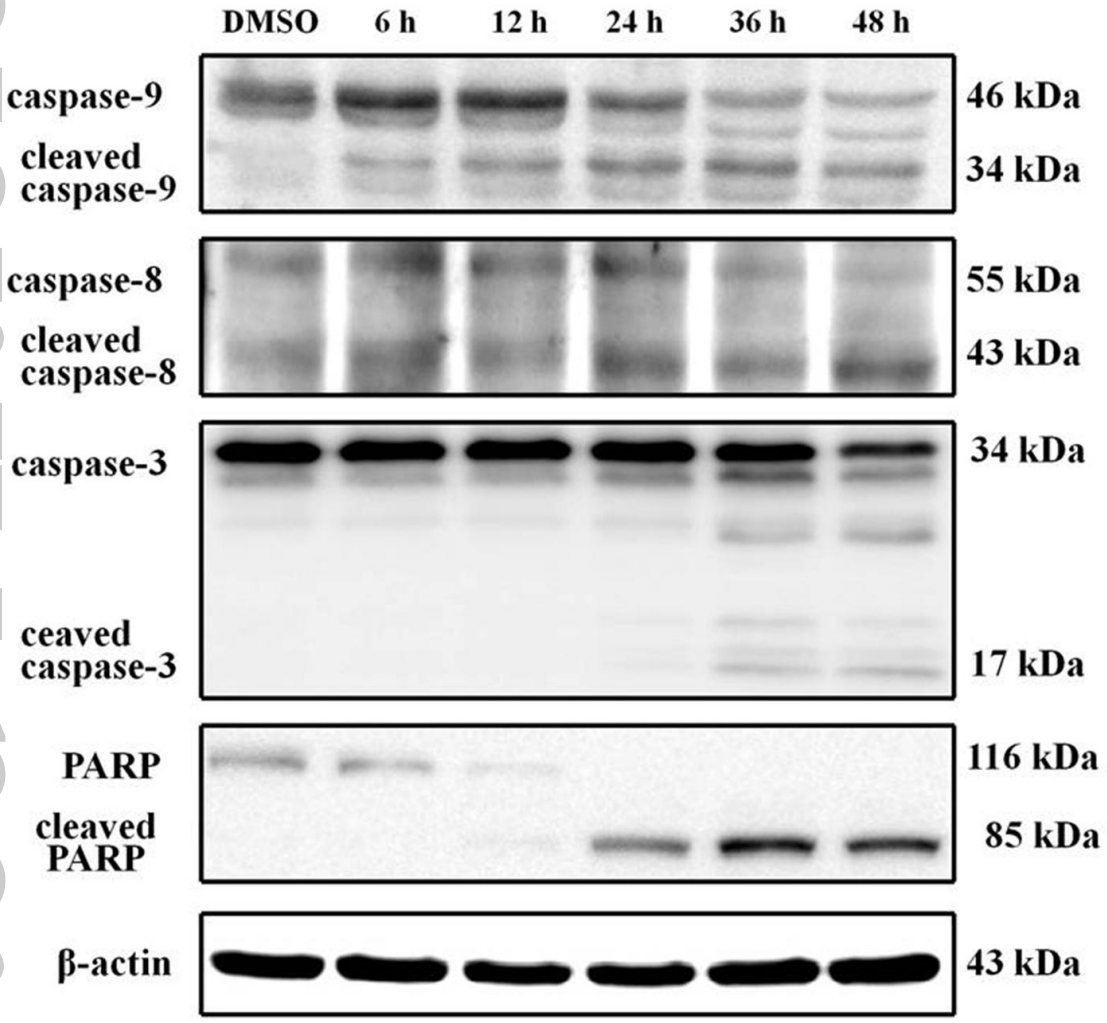

Fig. 10. Compound **11e** induced caspase-3, caspase-8, and caspase-9 activity in COLO 205 cells. COLO 205 cells were treated with 50 nM **11e** for the indicated times and lysed for protein extraction. Protein samples (40 μg protein/lane) were separated using 10% SDS-PAGE and subjected to immunoblotting with antibodies specific to caspase-9, caspase-8, caspase-3, PARP, and β-actin (n = 3 independent experiments). β-Actin was used as a loading control.

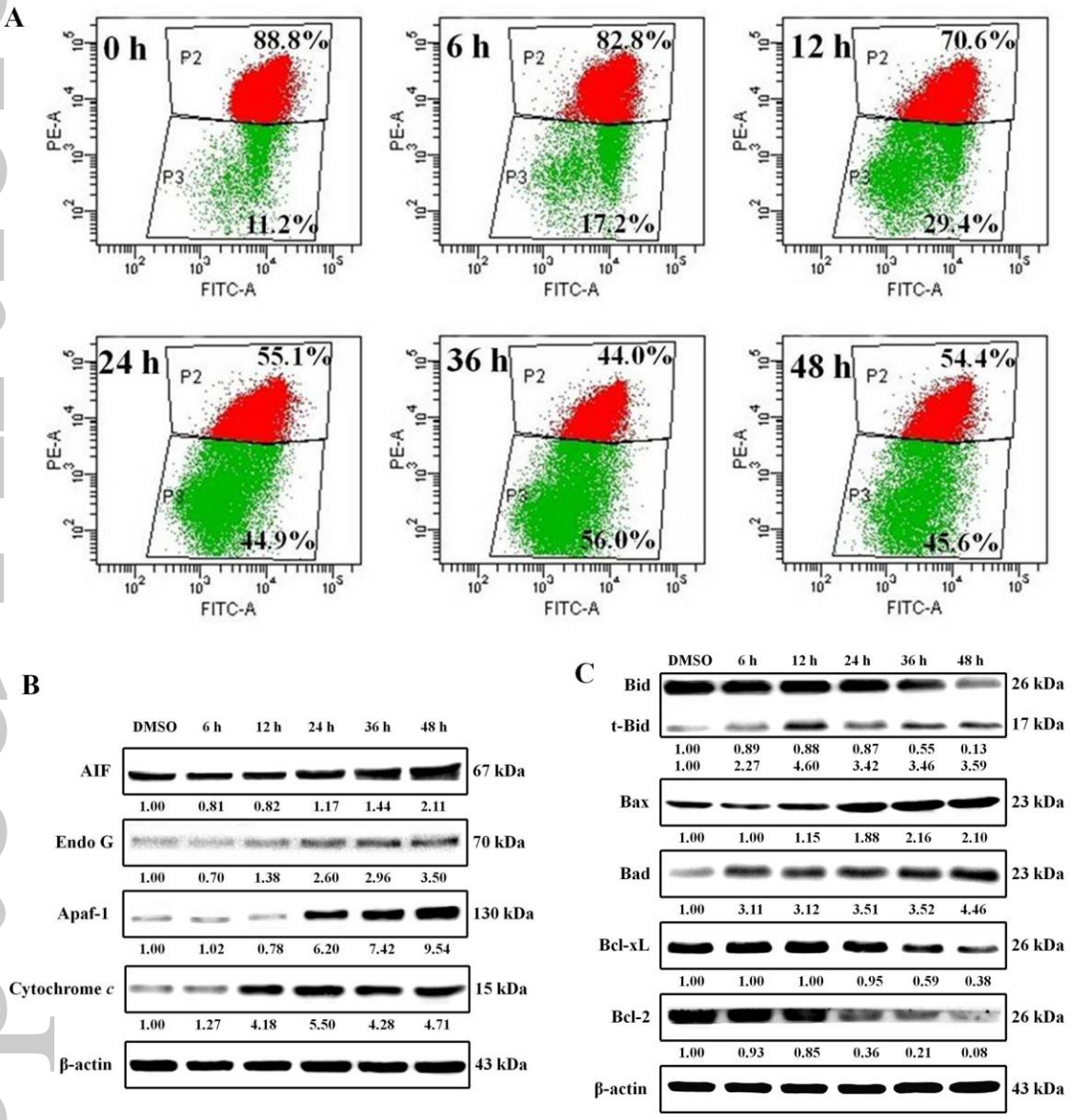

Fig. 11. Compound **11e** induced mitochondrial apoptosis pathway in COLO 205 cells. (A) Effects of **11e** on mitochondrial membrane potential in COLO 205 cells. Cells (1×10^6 cells/ml) were untreated or treated with **11e** (50 nM, 6-48 h) to induce apoptosis. Cells were stained with JC-1 according to the protocol on a BD™ MitoScreen as described in the section Methods for Staining Cells with JC-1 and Analyzing by Flow Cytometry. (B) COLO 205 cells were treated with 50 nM **11e** for the indicated times and lysed for protein extraction. Protein samples (40 μg protein/lane) were separated using 10% SDS-PAGE and subjected to immunoblotting with antibodies specific to AIF, Endo G, Apaf-1, cytochrome *c*, and β-actin (n = 3 independent experiments). (C) Compound **11e** affected

Bcl-2 family proteins in COLO 205 cells. COLO 205 cells were treated with 50 nM **11e** for the indicated times and lysed for protein extraction. Protein samples (40 μg protein/lane) were separated using 10% SDS-PAGE and subjected to immunoblotting with antibodies specific to Bid, Bax, Bad, Bcl-xL, Bcl-2, and β-actin (n = 3 independent experiments). β-Actin was used as a loading control.

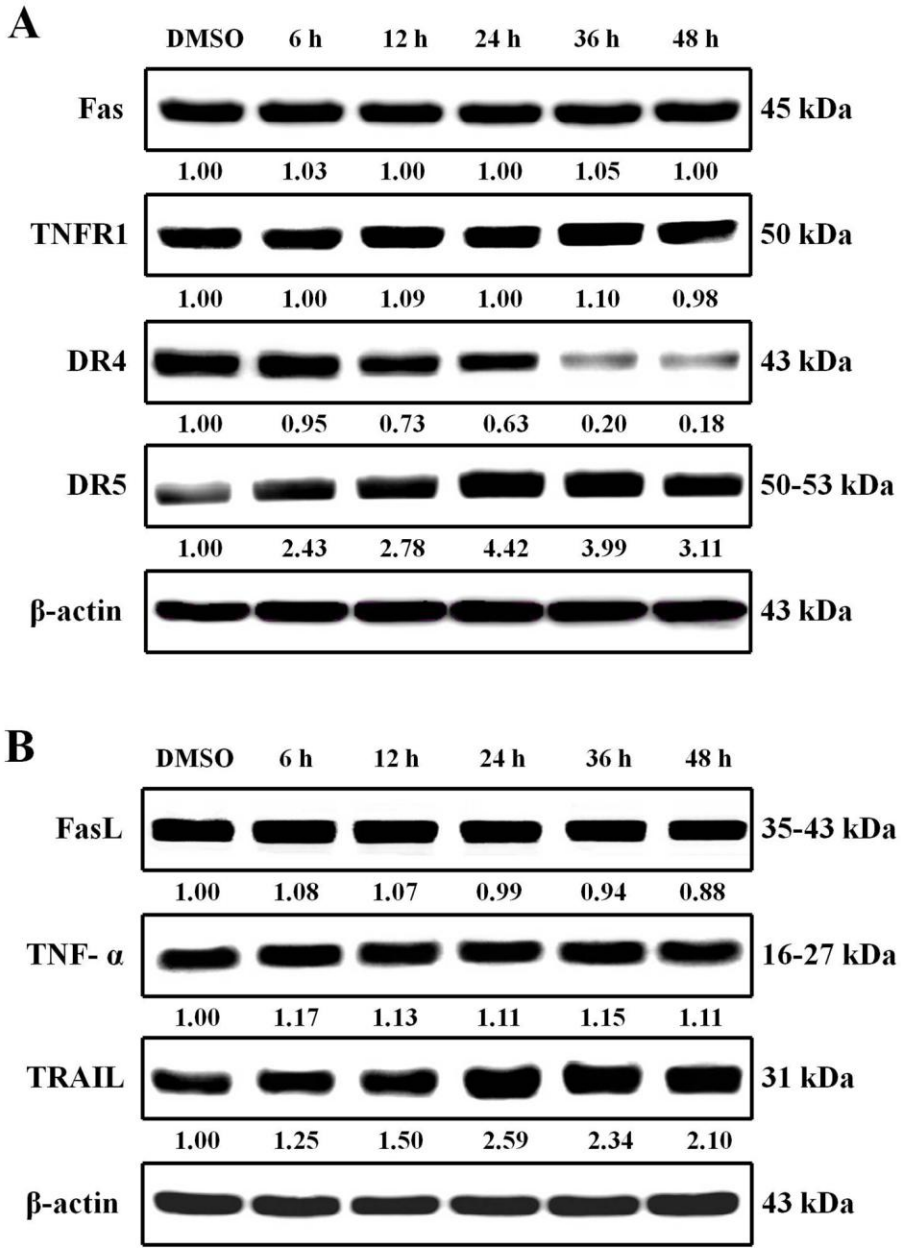

Fig. 12. Compound **11e** induced death receptor apoptosis pathway in COLO 205 cells. COLO 205 cells were treated with 50 nM **11e** for the indicated times and lysed for protein extraction. Protein samples (40 μg protein/lane) were separated using 10% SDS-PAGE and subjected to immunoblotting with antibodies specific to Fas, TNFR1, DR4, DR5 (A), FasL, TNF-α, TRAIL (B), and β-actin (n = 3 independent experiments). β-Actin was used as a loading control.

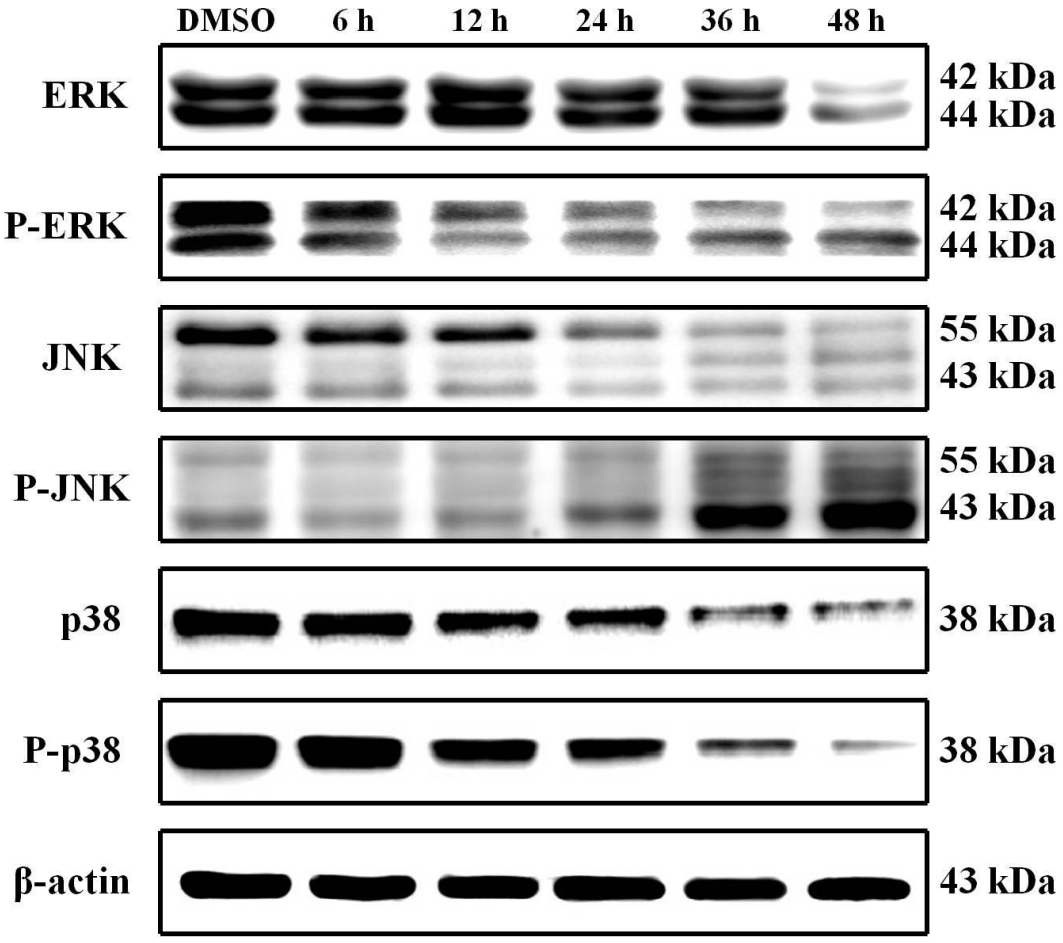

Fig. 13. Expression of MAPKs in the **11e**-treated COLO 205 cells. COLO 205 cells were treated with 50 nM **11e** for the indicated times and lysed for protein extraction. Protein samples (40 μg protein/lane) were separated using 10% SDS-PAGE and subjected to immunoblotting with antibodies specific to ERK1/2, phospho-ERK1/2, JNK, phospho-JNK, p38, phospho-p38 and β-actin (n = 3 independent experiments). β-Actin was used as a loading control.

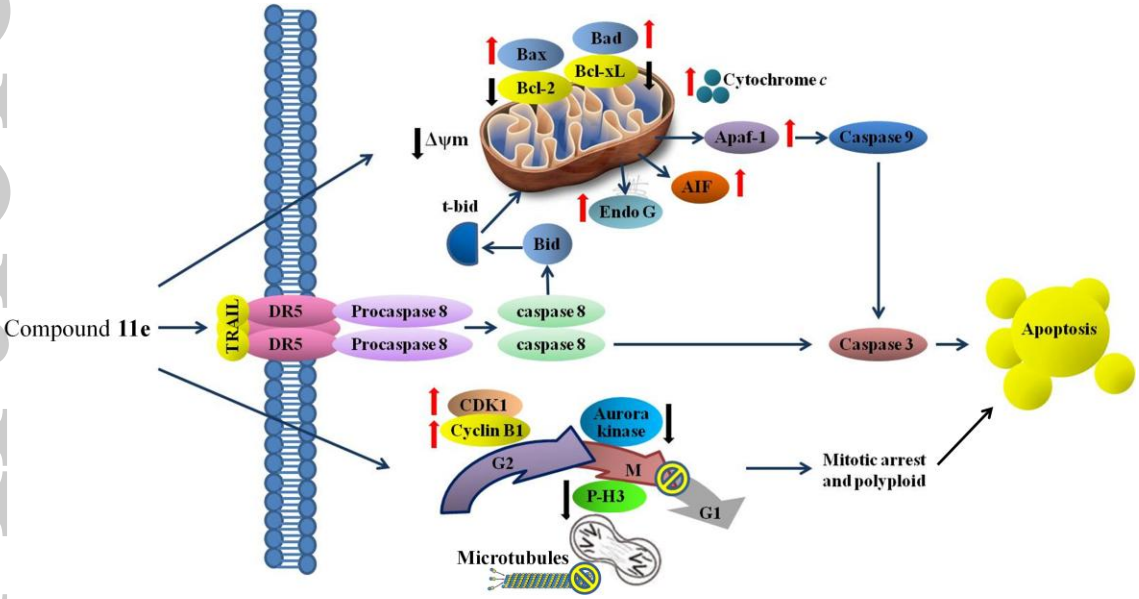

Fig. 14. The signaling pathways of **11e**-induced G2/M phase arrest and apoptosis in human colon cancer COLO 205 cells.

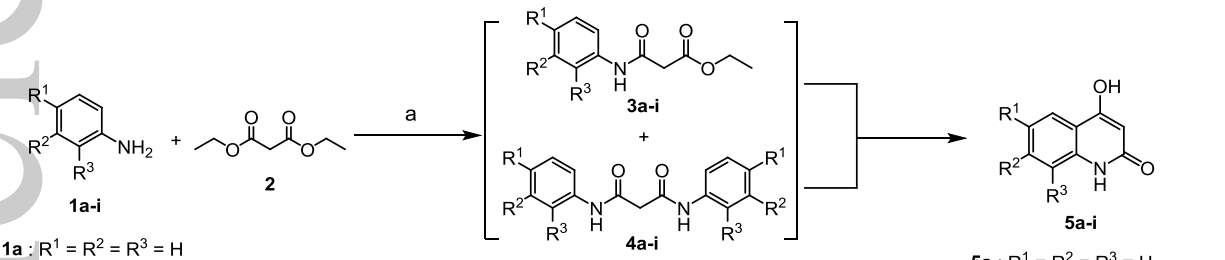

1a : $R^1 = R^2 = R^3 = H$
1b : $R^1 = F$, $R^2 = R^3 = H$
1c : $R^1 = Cl$, $R^2 = R^3 = H$
1d : $R^1 = CH_3$, $R^2 = R^3 = H$
1e : $R^1 = OCH_3$, $R^2 = R^3 = H$
1f : $R^1 = R^3 = H$, $R^2 = OCH_3$
1g : $R^1 = R^2 = H$, $R^3 = OCH_3$
1h : $R^1 = R^2 = H$, $R^3 = Cl$
1i : $R^1 = R^2 = H$, $R^3 = CH_3$

3a, **4a** : $R^1 = R^2 = R^3 = H$
3b, **4b** : $R^1 = F$, $R^2 = R^3 = H$
3c, **4c** : $R^1 = Cl$, $R^2 = R^3 = H$
3d, **4d** : $R^1 = CH_3$, $R^2 = R^3 = H$
3e, **4e** : $R^1 = OCH_3$, $R^2 = R^3 = H$
3f, **4f** : $R^1 = R^3 = H$, $R^2 = OCH_3$
3g, **4g** : $R^1 = R^2 = H$, $R^3 = OCH_3$
3h, **4h** : $R^1 = R^2 = H$, $R^3 = Cl$
3i, **4i** : $R^1 = R^2 = H$, $R^3 = CH_3$

5a : $R^1 = R^2 = R^3 = H$
5b : $R^1 = F$, $R^2 = R^3 = H$
5c : $R^1 = Cl$, $R^2 = R^3 = H$
5d : $R^1 = CH_3$, $R^2 = R^3 = H$
5e : $R^1 = OCH_3$, $R^2 = R^3 = H$
5f : $R^1 = R^3 = H$, $R^2 = OCH_3$
5g : $R^1 = R^2 = H$, $R^3 = OCH_3$
5h : $R^1 = R^2 = H$, $R^3 = Cl$
5i : $R^1 = R^2 = H$, $R^3 = CH_3$

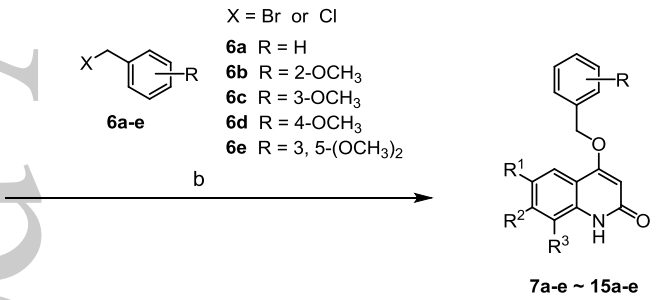

7a : $R^1 = R^2 = R^3 = H$; R = H
7b : $R^1 = R^2 = R^3 = H$; R = 2'-OCH_3
7c : $R^1 = R^2 = R^3 = H$; R = 3'-OCH_3
7d : $R^1 = R^2 = R^3 = H$; R = 4'-OCH_3
7e : $R^1 = R^2 = R^3 = H$; R = 3', 5'-$(OCH_3)_2$

8a : $R^1 = F$, $R^2 = R^3 = H$; R = H
8b : $R^1 = F$, $R^2 = R^3 = H$; R = 2'-OCH_3
8c : $R^1 = F$, $R^2 = R^3 = H$; R = 3'-OCH_3
8d : $R^1 = F$, $R^2 = R^3 = H$; R = 4'-OCH_3
8e : $R^1 = F$, $R^2 = R^3 = H$; R = 3', 5'-$(OCH_3)_2$

9a : $R^1 = Cl$, $R^2 = R^3 = H$; R = H
9b : $R^1 = Cl$, $R^2 = R^3 = H$; R = 2'-OCH_3
9c : $R^1 = Cl$, $R^2 = R^3 = H$; R = 3'-OCH_3
9d : $R^1 = Cl$, $R^2 = R^3 = H$; R = 4'-OCH_3
9e : $R^1 = Cl$, $R^2 = R^3 = H$; R = 3', 5'-$(OCH_3)_2$

10a : $R^1 = CH_3$, $R^2 = R^3 = H$; R = H
10b : $R^1 = CH_3$, $R^2 = R^3 = H$; R = 2'-OCH_3
10c : $R^1 = CH_3$, $R^2 = R^3 = H$; R = 3'-OCH_3
10d : $R^1 = CH_3$, $R^2 = R^3 = H$; R = 4'-OCH_3
10e : $R^1 = CH_3$, $R^2 = R^3 = H$; R = 3', 5'-$(OCH_3)_2$

11a : $R^1 = OCH_3$, $R^2 = R^3 = H$; R = H
11b : $R^1 = OCH_3$, $R^2 = R^3 = H$; R = 2'-OCH_3
11c : $R^1 = OCH_3$, $R^2 = R^3 = H$; R = 3'-OCH_3
11d : $R^1 = OCH_3$, $R^2 = R^3 = H$; R = 4'-OCH_3
11e : $R^1 = OCH_3$, $R^2 = R^3 = H$; R = 3', 5'-$(OCH_3)_2$

12a : $R^1 = R^3 = H$, $R^2 = OCH_3$; R = H
12b : $R^1 = R^3 = H$, $R^2 = OCH_3$; R = 2'-OCH_3
12c : $R^1 = R^3 = H$, $R^2 = OCH_3$; R = 3'-OCH_3
12d : $R^1 = R^3 = H$, $R^2 = OCH_3$; R = 4'-OCH_3
12e : $R^1 = R^3 = H$, $R^2 = OCH_3$; R = 3', 5'-$(OCH_3)_2$

13a : $R^1 = R^2 = H$, $R^3 = OCH_3$; R = H
13b : $R^1 = R^2 = H$, $R^3 = OCH_3$; R = 2'-OCH_3
13c : $R^1 = R^2 = H$, $R^3 = OCH_3$; R = 3'-OCH_3
13d : $R^1 = R^2 = H$, $R^3 = OCH_3$; R = 4'-OCH_3
13e : $R^1 = R^2 = H$, $R^3 = OCH_3$; R = 3', 5'-$(OCH_3)_2$

14a : $R^1 = R^2 = H$, $R^3 = Cl$; R = H
14b : $R^1 = R^2 = H$, $R^3 = Cl$; R = 2'-OCH_3
14c : $R^1 = R^2 = H$, $R^3 = Cl$; R = 3'-OCH_3
14d : $R^1 = R^2 = H$, $R^3 = Cl$; R = 4'-OCH_3
14e : $R^1 = R^2 = H$, $R^3 = Cl$; R = 3', 5'-$(OCH_3)_2$

15a : $R^1 = R^2 = H$, $R^3 = CH_3$; R = H
15b : $R^1 = R^2 = H$, $R^3 = CH_3$; R = 2'-OCH_3
15c : $R^1 = R^2 = H$, $R^3 = CH_3$; R = 3'-OCH_3
15d : $R^1 = R^2 = H$, $R^3 = CH_3$; R = 4'-OCH_3
15e : $R^1 = R^2 = H$, $R^3 = CH_3$; R = 3', 5'-$(OCH_3)_2$

Scheme 1. Reagents and conditions: (a) 130 °C with PPA. (b) K_2CO_3/DMF, 80-90 °C.

Table 1. Anti-proliferative effects of compounds **7a–e~15a–e**.

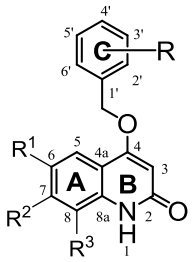

Compd	R^1	R^2	R^3	R	IC_{50} (μM) [a]				
					HL-60 [b]	Hep 3B [b]	H460 [b]	COLO205 [b]	Detroit 551 [b]
7a	H	H	H	H	> 50	> 50	> 50	> 50	> 50
7b	H	H	H	2'-OCH_3	> 50	> 50	> 50	> 50	> 50
7c	H	H	H	3'-OCH_3	16.4	> 50	> 50	7.5	> 50
7d	H	H	H	4'-OCH_3	> 50	> 50	> 50	> 50	> 50
7e	H	H	H	3', 5'-$(OCH_3)_2$	0.68	0.64	0.69	0.42	> 50
8a	F	H	H	H	> 50	> 50	> 50	> 50	> 50
8b	F	H	H	2'-OCH_3	8.7	> 50	> 50	7.3	> 50
8c	F	H	H	3'-OCH_3	> 50	> 50	> 50	50	> 50
8d	F	H	H	4'-OCH_3	> 50	> 50	> 50	> 50	> 50
8e	F	H	H	3', 5'-$(OCH_3)_2$	0.4	0.9	0.6	0.39	> 50
9a	Cl	H	H	H	4.5	> 50	> 50	9.8	> 50
9b	Cl	H	H	2'-OCH_3	0.6	2.2	2.8	0.41	> 50
9c	Cl	H	H	3'-OCH_3	0.3	0.8	1.0	0.35	> 50
9d	Cl	H	H	4'-OCH_3	> 50	> 50	> 50	> 50	> 50
9e	Cl	H	H	3', 5'-$(OCH_3)_2$	0.0295	0.15	0.19	0.054	> 50
10a	CH_3	H	H	H	–	> 50	> 50	8.2	–
10b	CH_3	H	H	2'-OCH_3	–	1.8	1.7	1.0	–
10c	CH_3	H	H	3'-OCH_3	–	0.68	0.89	0.36	–
10d	CH_3	H	H	4'-OCH_3	–	> 50	> 50	> 50	–
10e	CH_3	H	H	3', 5'-$(OCH_3)_2$	–	0.54	0.27	0.06	–
11a	OCH_3	H	H	H	8.5	27.0	51.7	8.8	> 50
11b	OCH_3	H	H	2'-OCH_3	1.5	4.3	3.3	5.0	> 50
11c	OCH_3	H	H	3'-OCH_3	0.2	0.9	0.6	0.21	> 50
11d	OCH_3	H	H	4'-OCH_3	> 50	> 50	> 50	> 50	> 50
11e	OCH_3	H	H	3', 5'-$(OCH_3)_2$	0.014	0.035	0.04	0.028	> 50
12a	H	OCH_3	H	H	–	9.55	17.3	14.2	–
12b	H	OCH_3	H	2'-OCH_3	–	4.02	7.1	6.4	–
12c	H	OCH_3	H	3'-OCH_3	–	3.23	> 50	8.2	–
12d	H	OCH_3	H	4'-OCH_3	–	> 50	> 50	> 50	–
12e	H	OCH_3	H	3', 5'-$(OCH_3)_2$	–	2.11	3.96	4.9	–
13a	H	H	OCH_3	H	> 50	> 50	> 50	34.1	> 50
13b	H	H	OCH_3	2'-OCH_3	> 50	> 50	> 50	> 50	> 50
13c	H	H	OCH_3	3'-OCH_3	20.0	39.9	32.3	22.6	> 50
13d	H	H	OCH_3	4'-OCH_3	> 50	> 50	> 50	> 50	> 50
13e	H	H	OCH_3	3', 5'-$(OCH_3)_2$	3.3	3.8	2.2	2.6	> 50
14a	H	H	Cl	H	–	> 50	> 50	> 50	–
14b	H	H	Cl	2'-OCH_3	–	> 50	> 50	> 50	–
14c	H	H	Cl	3'-OCH_3	–	> 50	> 50	> 50	–
14d	H	H	Cl	4'-OCH_3	–	> 50	> 50	> 50	–
14e	H	H	Cl	3', 5'-$(OCH_3)_2$	–	3.64	19.4	9.7	–
15a	H	H	CH_3	H	> 50	> 50	> 50	> 50	> 50

15b	H	H	CH_3	2'-OCH_3	20.0	> 50	> 50	41.5	> 50
15c	H	H	CH_3	3'-OCH_3	> 50	> 50	> 50	> 50	> 50
15d	H	H	CH_3	4'-OCH_3	10.0	> 50	> 50	> 50	> 50
15e	H	H	CH_3	3', 5'-$(OCH_3)_2$	0.72	2.0	3.3	2.6	> 50
etoposide					5.48	–	1.0	–	–

[a]Human tumor cells were treated with different concentrations of samples for 48 h. Data are presented as IC_{50} (μM, the concentration of 50% proliferation-inhibitory effect). [b] Cell lines include leukemia (HL-60), liver carcinoma (Hep3B), lung carcinoma (H460), colon carcinoma (COLO205), and normalskin fibroblast (Detroit 551).

Table 2. Growth percentages of selected compounds in the NCI *in vitro* 60-cell Drug Screen Program.

Panel/Cell line	Compounds /Growth percentage (%) [a]			
	9b	**9c**	**9e**	**11e**
Leukemia				
CCRF-CEM	18.56	11.98	15.94	**–26.21** [b]
HL-60(TB)	9.64	**–9.34**	7.37	**–32.61**
K-562	15.80	17.65	11.80	3.56
MOLT-4	39.79	38.04	42.35	4.78
RPMI-8226	19.77	17.87	15.90	**–6.67**
SR	14.68	5.97	7.02	**–4.86**
Non-small cell lung cancer				
A549/ATCC	29.44	21.67	**–22.24**	7.15
EKVX	50.93	41.72	52.28	–
HOP-62	**–18.38**	**–22.55**	**–27.19**	24.70
HOP-92	19.45	46.83	43.66	28.92
NCI-H226	42.44	48.35	8.57	54.52
NCI-H23	32.69	33.31	3.47	**–47.65**
NCI-H322M	36.63	35.35	39.53	21.59
NCI-H460	10.03	5.68	2.71	3.87
NCI-H522	18.21	22.30	**–0.77**	**–29.70**
Colon cancer				
COLO 205	**–55.40**	**–57.40**	**–64.41**	**–59.50**
HCC-2998	23.46	27.86	**–12.73**	**–32.77**
HCT-116	25.11	28.76	3.95	0.12
HCT-15	24.78	19.69	17.60	7.24
HT-29	7.13	2.57	0.32	**–27.36**
KM12	30.65	22.39	10.66	1.77
SW-620	12.10	21.07	20.17	10.28
CNS cancer				
SF-268	42.91	42.47	27.59	8.61
SF-295	6.76	9.92	**–2.30**	**–3.44**
SF-539	5.03	**–2.10**	**–35.52**	**–28.70**
SNB-19	28.95	30.82	19.73	48.02
SNB-75	**–22.87**	**–16.82**	**–42.27**	–
U251	16.38	18.14	**–21.80**	5.44
Melanoma				
LOX IMVI	14.48	17.90	2.15	**–6.75**
MALME-3M	45.00	31.84	32.02	55.33
M14	13.96	19.46	8.30	**–50.76**
MDA-MB-435	**–46.28**	**–43.14**	**–43.16**	**–41.44**
SK-MEL-2	23.93	5.30	10.59	**–14.08**
SK-MEL-28	**–12.04**	4.07	**–8.81**	7.02
SK-MEL-5	**–25.75**	**–32.70**	0.36	**–27.48**
UACC-257	24.32	21.96	19.86	34.86
UACC-62	**–19.98**	4.59	5.49	**–48.21**
Ovarian cancer				
IGROV1	45.21	39.68	46.14	–
OVCAR-3	4.64	6.22	**–59.96**	**–32.89**
OVCAR-4	34.25	42.73	29.48	40.39
OVCAR-5	48.30	36.30	32.38	18.06
OVCAR-8	33.86	24.06	6.15	9.94
NCI/ADR-RES	19.48	20.52	3.42	**–14.04**
SK-OV-3	**–17.68**	**–27.16**	**–27.00**	**–0.80**
Renal cancer				
786-0	33.73	39.62	3.94	**–2.61**
A498	21.88	16.02	**–2.40**	**–8.21**
ACHN	44.36	43.14	23.77	19.79
CAKI-1	31.23	30.29	27.34	9.52
RXF 393	**–14.00**	–	**–25.73**	**–11.48**
SN12C	27.70	32.18	16.82	2.52
TK-10	50.99	41.50	**–2.79**	18.32
UO-31	38.23	34.68	28.46	30.52
Prostate cancer				
PC-3	21.26	23.95	27.74	20.50
DU-145	16.06	14.85	20.65	1.31
Breast cancer				
MCF7	**–5.90**	1.34	**–35.96**	13.94
MDA-MB-231/ATCC	29.63	40.04	5.25	**–2.71**
HS 578T	9.12	21.68	21.06	31.90
BT-549	42.21	48.16	30.87	**–19.04**
T-47D	**–19.71**	**–16.85**	21.81	50.59
MDA-MB-468	24.05	**–25.33**	**–23.96**	**–4.24**
Mean growth	17.02	16.59	5.26	0.19
Range of growth	**–55.40** to 50.99	**–57.40** to 48.35	**–64.41** to 52.28	**–59.50** to 55.33

The most sensitive cell line	COLO 205(Colon cancer)	COLO 205(Colon cancer)	COLO 205(Colon cancer)	COLO 205(Colon cancer)
Positive cytostatic effect [c]	47/60	49/59	41/60	28/57
Positive cytotoxic effect [d]	11/60	10/59	18/60	26/57

[a]Data obtained from NCI *in vitro*60-cell screen program at 10 μM. [b]Negative valuesrepresent compound proved lethal to the cancer cell line (cell death). [c]Ratio between number of cell lines with percent growth from 0 to 50 and total number of cell lines. [d]Ratio between number of cell lines with percent growth of < 0 and total number of cell lines.

Table 3. *In vitro* antitumor activity (GI_{50} in μM), toxicity (LC_{50} in μM), and TGI data of selected compounds **9b**, **9c**, **9e** and **11e**.

Panel/Cell line	Compounds [a]														
	9b			**9c**			**9e**			**11e**			5-FU [b]		
	GI_{50}	TGI	LC_{50}	GI_{50}	TGI	LC_{50}	GI_{50}	TGI	LC_{50}	GI_{50}	TGI	LC_{50}	GI_{50}	TGI	LC_{50}
Leukemia															
CCRF-CEM	0.39	19.50	>100	0.31	>100	>100	0.04	>100	>100	0.03	>100	>100	10.00	>100	>100
HL-60(TB)	–	–	–	–	–	–	–	–	–	0.04	>100	>100	2.51	>100	>100
K-562	0.08	11.60	92.50	0.03	–	>100	**<0.01**	1.67	>100	**<0.01**	>100	>100	3.98	>100	>100
MOLT-4	0.51	32.50	>100	0.33	>100	>100	0.05	>100	>100	0.07	>100	>100	0.32	50.12	>100
RPMI-8226	0.61	21.40	>100	0.43	>100	>100	0.08	>100	>100	0.03	>100	>100	0.05	50.12	>100
SR	0.20	0.89	>100	0.03	0.95	>100	**<0.01**	0.08	>100	**<0.01**	>100	>100	0.03	10.00	>100
Non-small cell lung cancer															
A549/ATCC	–	–	–	–	–	–	–	–	–	0.02	>100	>100	0.20	63.10	>100
EKVX	0.46	40.70	>100	0.22	>100	>100	0.24	>100	>100	–	–	–	63.10	>100	>100
HOP-62	0.53	2.82	17.80	0.33	–	>100	0.04	14.10	43.30	0.03	12.20	75.10	0.40	>100	>100
HOP-92	1.09	5.18	31.80	1.42	>100	>100	11.90	>100	>100	0.02	10.80	>100	79.43	>100	>100
NCI-H226	2.24	41.00	>100	3.25	>100	>100	10.20	>100	>100	2.80	>100	>100	50.12	>100	>100
NCI-H23	0.93	12.00	69.40	0.51	>100	>100	0.08	63.80	>100	0.07	13.30	>100	0.32	39.81	>100
NCI-H322M	0.57	9.76	>100	0.36	>100	>100	0.05	>100	>100	0.08	>100	>100	0.20	7.94	>100
NCI-H460	0.39	3.87	37.10	0.05	–	>100	0.03	23.90	>100	0.03	>100	>100	0.06	50.12	>100
NCI-H522	0.15	0.46	6.55	0.03	0.19	12.30	**<0.01**	0.03	0.10	**<0.01**	0.03	>100	7.94	63.10	>100
Colon cancer															
COLO 205	0.39	2.45	60.80	0.22	1.89	>100	0.03	0.10	2.48	**<0.01**	0.03	0.09	0.16	63.10	>100
HCC-2998	1.04	12.40	61.10	0.30	>100	>100	0.12	31.60	>100	0.05	1.98	>100	0.05	39.81	>100
HCT-116	0.42	1.74	6.74	0.11	–	–	0.04	>100	>100	0.04	10.40	>100	0.25	3.98	25.12
HCT-15	0.54	>100	>100	0.29	>100	>100	0.04	>100	>100	0.03	18.90	>100	0.10	50.12	>100
HT-29	0.30	0.85	11.50	0.04	0.41	–	0.03	0.08	>100	0.01	–	>100	0.16	63.10	>100
KM12	0.53	18.10	>100	0.06	>100	>100	0.04	>100	>100	0.03	3.18	>100	0.20	39.81	>100
SW-620	0.39	12.50	>100	0.05	>100	>100	0.03	>100	>100	0.02	>100	>100	1.00	>100	>100
CNS cancer															
SF-268	0.68	20.60	>100	0.49	>100	>100	0.05	75.20	>100	1.08	>100	>100	1.58	>100	>100
SF-295	0.24	0.74	5.10	0.09	0.77	4.63	0.02	0.08	24.90	–	–	–	0.25	3.98	>100
SF-539	0.60	2.77	14.00	0.39	2.21	>100	0.04	1.20	>100	0.03	0.21	58.70	0.06	79.43	>100
SNB-19	0.58	14.30	>100	0.41	4.49	>100	0.06	28.30	>100	0.09	>100	>100	3.98	79.43	>100
SNB-75	0.30	1.40	14.80	0.24	0.95	13.50	0.03	0.09	36.90	0.01	0.05	26.70	79.43	>100	>100
U251	0.45	10.50	46.80	0.42	3.57	>100	0.05	16.00	56.60	0.04	12.00	>100	1.00	79.43	>100
Melanoma															
LOX IMVI	0.59	3.58	32.70	0.51	2.78	>100	0.07	>100	>100	0.06	10.30	>100	0.25	50.12	79.43
MALME-3M	0.32	10.30	>100	0.11	>100	>100	0.03	54.30	>100	–	>100	>100	0.05	2.51	>100
M14	0.32	1.11	57.90	0.14	1.25	>100	0.04	2.07	>100	0.04	0.26	4.29	1.00	>100	>100
MDA-MB-435	0.06	0.24	0.73	0.02	0.04	0.09	**<0.01**	0.02	0.08	**<0.01**	0.02	2.68	0.08	79.43	>100

SK-MEL-2	0.34	0.86	25.40	0.15	0.74	>100	0.02	0.06	27.20	–	>100	>100	63.10	>100	>100
SK-MEL-28	0.71	12.70	>100	0.47	>100	>100	0.07	>100	>100	0.07	>100	>100	1.00	63.10	>100
SK-MEL-5	0.26	–	54.70	0.19	–	>100	0.03	>100	>100	0.02	1.85	7.08	0.50	39.81	79.43
UACC-257	–	>100	>100	–	>100	>100	–	>100	>100	8.08	>100	>100	3.98	79.43	>100
UACC-62	0.45	4.25	30.80	0.35	8.90	>100	0.04	51.60	>100	0.03	>100	>100	0.50	39.81	>100
Ovarian cancer															
IGROV1	0.56	6.57	48.60	0.35	>100	>100	0.06	64.80	>100	0.42	>100	>100	1.26	31.62	>100
OVCAR-3	0.38	1.36	7.54	0.24	1.17	5.06	0.02	0.07	7.79	0.02	0.07	28.60	0.02	0.32	50.12
OVCAR-4	2.77	39.80	>100	0.96	>100	>100	0.83	>100	>100	1.11	>100	>100	3.98	79.43	>100
OVCAR-5	2.01	22.80	>100	1.90	>100	>100	0.32	>100	>100	0.09	69.50	>100	10.00	50.12	>100
OVCAR-8	0.48	13.20	57.00	0.43	>100	>100	0.06	28.30	>100	0.05	>100	>100	1.58	31.62	>100
NCI/ADR-RES	0.37	8.09	79.50	0.08	–	>100	0.03	11.70	>100	0.01	24.60	>100	0.32	12.59	>100
SK-OV-3	0.50	2.30	11.70	0.35	2.10	>100	0.03	1.04	96.90	0.03	0.93	64.20	19.95	63.10	>100
Renal cancer															
786-0	0.62	2.51	8.27	0.58	–	>100	0.07	32.30	>100	1.15	11.40	>100	0.79	50.12	>100
A498	0.45	1.87	6.10	0.16	1.88	>100	0.03	22.30	>100	0.02	0.09	78.10	0.40	>100	>100
ACHN	0.73	4.47	31.40	0.61	>100	>100	0.06	>100	>100	0.08	>100	>100	0.32	31.62	>100
CAKI-1	0.32	3.55	52.50	0.06	–	>100	0.03	>100	>100	0.02	>100	>100	0.08	2.00	>100
RXF 393	0.47	2.58	13.70	0.41	3.14	>100	0.05	0.31	36.30	0.02	0.08	>100	2.51	31.62	>100
SN12C	0.67	20.80	>100	0.67	>100	>100	0.10	>100	>100	0.09	>100	>100	0.50	25.12	>100
TK-10	–	–	–	–	–	–	–	–	–	1.05	75.80	>100	1.26	79.43	>100
UO-31	0.39	2.36	15.50	0.16	>100	>100	0.04	>100	>100	0.08	>100	>100	1.58	50.12	>100
Prostate cancer															
PC-3	0.89	24.10	>100	0.71	>100	>100	0.06	>100	>100	0.02	>100	>100	2.51	>100	>100
DU-145	0.56	13.70	>100	0.33	–	>100	0.04	29.30	>100	0.04	16.00	>100	0.40	>100	>100
Breast cancer															
MCF7	0.57	12.30	78.90	0.32	>100	>100	0.21	>100	>100	0.03	>100	>100	0.08	50.12	>100
MDA-MB-231/ATCC	0.92	10.10	58.50	1.29	>100	>100	0.15	55.50	>100	0.15	26.20	>100	6.31	39.81	>100
HS 578T	0.57	5.97	>100	0.30	2.89	>100	0.03	16.80	>100	0.02	100	>100	10.00	>100	>100
BT-549	0.74	19.60	>100	0.65	>100	>100	–	60.00	>100	0.20	9.26	>100	10.00	>100	>100
T-47D	0.51	7.23	38.20	0.38	>100	>100	–	>100	>100	0.04	>100	>100	7.94	50.12	>100
MDA-MB-468	1.73	6.13	29.70	0.29	1.03	>100	0.21	0.61	>100	0.05	0.41	>100	–	–	–

[a]Data obtained from NCI's in vitro disease-oriented human tumor cell lines screen. [b] NCI data for 5-FU: NSC 19893. (NCI Anti-cancer Screening Program; http://dtp.nci.nih.gov/docs/cancer/searches/standard_mechanism_list.html).

Table 4. Median growth inhibitory concentration (GI_{50}, μM) and GI_{50} selectivity ratios of selected compounds in the NCI *in vitro* 60-cell Drug Screen Program.

Subpanel tumor Cell lines	Compounds							
	9b (NSC 756950)		**9c (NSC 756949)**		**9e (NSC 756951)**		**11e (NSC 764592)**	
	Subpanel MID [b] (μM)	Selectivity Ratio [c]	Subpanel MID [b] (μM)	Selectivity Ratio [c]	Subpanel MID [b] (μM)	Selectivity Ratio [c]	Subpanel MID [b] (μM)	Selectivity Ratio [c]
Leukemia	0.36	1.74	0.23	1.86	0.06	7.56	0.04	7.36
Non-small cell lung cancer	0.80	0.79	0.77	0.55	3.22	0.13	0.44	0.72
Colon cancer	0.52	1.21	0.15	2.75	0.05	9.09	0.03	10.42
CNS cancer	0.48	1.31	0.34	1.24	0.04	10.28	0.25	1.25
Melanoma	0.38	1.64	0.24	1.73	0.04	10.00	1.38	0.23
Ovarian cancer	1.01	0.62	0.62	0.68	0.19	2.22	0.25	1.27
Renal cancer	0.52	1.20	0.38	1.11	0.05	7.89	0.31	1.00
Prostate cancer	0.73	0.86	0.52	0.81	0.05	8.57	0.03	10.42
Breast cancer	0.84	0.74	0.54	0.78	0.15	2.86	0.08	3.83
Total MID [a]	0.62		0.42		0.43		0.31	
Average Selectivity Ratio		1.12		1.28		6.51		4.05

Total MID[a] = average sensitivity of all cell line in μM. Subpanel MID[b]= average sensitivity of individual subpanel cell lines in μM.

[c] Selectivity Ratio: Total MID[a] / Subpanel MID[b].